



NAVAL POSTGRADUATE SCHOOL

MONTEREY, CALIFORNIA

THESIS

**MINIMUM-ENERGY FLIGHT PATHS FOR UAVS USING
MESOSCALE WIND FORECASTS AND APPROXIMATE
DYNAMIC PROGRAMMING**

by

Gil Nachmani

December 2007

Thesis Advisor:
Second Reader:

Johannes O. Royset
Kevin Jones

Approved for public release; distribution is unlimited.

THIS PAGE INTENTIONALLY LEFT BLANK

REPORT DOCUMENTATION PAGE			<i>Form Approved OMB No. 0704-0188</i>	
Public reporting burden for this collection of information is estimated to average 1 hour per response, including the time for reviewing instruction, searching existing data sources, gathering and maintaining the data needed, and completing and reviewing the collection of information. Send comments regarding this burden estimate or any other aspect of this collection of information, including suggestions for reducing this burden, to Washington headquarters Services, Directorate for Information Operations and Reports, 1215 Jefferson Davis Highway, Suite 1204, Arlington, VA 22202-4302, and to the Office of Management and Budget, Paperwork Reduction Project (0704-0188) Washington DC 20503.				
1. AGENCY USE ONLY (Leave blank)		2. REPORT DATE December 2007	3. REPORT TYPE AND DATES COVERED Master's Thesis	
4. TITLE AND SUBTITLE Minimum-Energy Flight Paths for UAVs Using Mesoscale Wind Forecasts and Approximate Dynamic Programming			5. FUNDING NUMBERS	
6. AUTHOR(S) Gil Nachmani				
7. PERFORMING ORGANIZATION NAME(S) AND ADDRESS(ES) Naval Postgraduate School Monterey, CA 93943-5000			8. PERFORMING ORGANIZATION REPORT NUMBER	
9. SPONSORING /MONITORING AGENCY NAME(S) AND ADDRESS(ES) N/A			10. SPONSORING/MONITORING AGENCY REPORT NUMBER	
11. SUPPLEMENTARY NOTES The views expressed in this thesis are those of the author and do not reflect the official policy or position of the Department of Defense or the U.S. Government.				
12a. DISTRIBUTION / AVAILABILITY STATEMENT Approved for public release; distribution is unlimited			12b. DISTRIBUTION CODE	
13. ABSTRACT <p>Fuel or battery consumption of unmanned aerial vehicles (UAVs) can be improved by utilizing or avoiding air currents. This thesis adopts a network modeling approach to formulate the problem of finding minimum energy flight paths. The relevant airspace is divided into small regions using a grid of nodes, inter-connected by arcs. A function, representing energy cost, is defined on every arc in terms of the solution of a constrained nonlinear program for the optimal local airspeed to fly in a given wind field. Then, shortest-path models are implemented on the network to find the optimal paths from an origin to a destination. Five models are studied and they correspond to cases of pre-planning of flight routes and dynamic updating of routes during the course of the flight. These models use three-dimensional grids of forecasted wind currents, produced by the Naval Research Laboratory's Coupled Ocean-Atmosphere Mesoscale Prediction System (COAMPS) with horizontal resolution of 1 km. One of the shortest-path models, a stochastic-dynamic model, assumes real-time measurement capabilities of the wind velocity in the vicinity of the UAV, through its GPS-INS system, and provides updated waypoints to follow after every measurement. For each model, the energy costs of the shortest-path solutions for 1000 randomized missions over a Nevada test site are simulated and compared to the energy costs of straight-line paths. For a 100 kg UAV, the dynamic model produces an average reduction of 15.1% in the energy consumption along 40 km long round trips, and an average reduction of 30.1% under windy conditions with average wind speeds larger than 15 m/s. A stochastic-dynamic model for maximum duration, solved using a heuristic algorithm, achieves an average increase of 32.2% in the flight duration for a 100 kg UAV.</p>				
14. SUBJECT TERMS Optimization, Unmanned Aerial Vehicles, Stochastic-Dynamic Shortest Path, Weather Forecasts, Aerodynamics, Correlation Structure.			15. NUMBER OF PAGES 85	
			16. PRICE CODE	
17. SECURITY CLASSIFICATION OF REPORT Unclassified	18. SECURITY CLASSIFICATION OF THIS PAGE Unclassified	19. SECURITY CLASSIFICATION OF ABSTRACT Unclassified	20. LIMITATION OF ABSTRACT UU	

NSN 7540-01-280-5500

Standard Form 298 (Rev. 2-89)
Prescribed by ANSI Std. Z39-18

THIS PAGE INTENTIONALLY LEFT BLANK

Approved for public release; distribution is unlimited.

**MINIMUM-ENERGY FLIGHT PATHS FOR UAVS USING MESOSCALE WIND
FORECASTS AND APPROXIMATE DYNAMIC PROGRAMMING**

Gil Nachmani
Captain, Israel Defense Forces
B.Sc., Hebrew University of Jerusalem, 2001

Submitted in partial fulfillment of the
requirements for the degree of

MASTER OF SCIENCE IN OPERATIONS RESEARCH

from the

**NAVAL POSTGRADUATE SCHOOL
December 2007**

Author: Gil Nachmani

Approved by: Johannes O. Royset
Thesis Advisor

Kevin Jones
Second Reader

James N. Eagle
Chairman, Department of Operations Research

THIS PAGE INTENTIONALLY LEFT BLANK

ABSTRACT

Fuel or battery consumption of unmanned aerial vehicles (UAVs) can be improved by utilizing or avoiding air currents. This thesis adopts a network modeling approach to formulate the problem of finding minimum energy flight paths. The relevant airspace is divided into small regions using a grid of nodes, inter-connected by arcs. A function, representing energy cost, is defined on every arc in terms of the solution of a constrained nonlinear program for the optimal local airspeed to fly in a given wind field. Then, shortest-path models are implemented on the network to find the optimal paths from an origin to a destination. Five models are studied and they correspond to cases of pre-planning of flight routes and dynamic updating of routes during the course of the flight. These models use three-dimensional grids of forecasted wind currents, produced by the Naval Research Laboratory's Coupled Ocean-Atmosphere Mesoscale Prediction System (COAMPS) with horizontal resolution of 1 km. One of the shortest-path models, a stochastic-dynamic model, assumes real-time measurement capabilities of the wind velocity in the vicinity of the UAV, through its GPS-INS system, and provides updated waypoints to follow after every measurement. For each model, the energy costs of the shortest-path solutions for 1000 randomized missions over a Nevada test site are simulated and compared to the energy costs of straight-line paths. For a 100 kg UAV, the dynamic model produces an average reduction of 15.1% in the energy consumption along 40 km long round trips, and an average reduction of 30.1% under windy conditions with average wind speeds larger than 15 m/s. A stochastic-dynamic model for maximum duration, solved using a heuristic algorithm, achieves an average increase of 32.2% in the flight duration for a 100 kg UAV.

THIS PAGE INTENTIONALLY LEFT BLANK

TABLE OF CONTENTS

I.	INTRODUCTION.....	1
A.	MOTIVATION	1
B.	THESIS OBJECTIVE AND SCOPE.....	1
C.	POTENTIAL BENEFITS OF THE STUDY.....	2
D.	RELATED WORK.....	2
E.	THESIS ORGANIZATION.....	3
II.	WIND AND FORECASTS.....	5
A.	CHAPTER OVERVIEW	5
B.	WIND BEHAVIOR	5
C.	WIND DATA.....	7
D.	MESOSCALE WEATHER FORECASTS	9
E.	USING FORECASTED WIND FIELDS.....	11
F.	TEMPORAL AND SPATIAL CORRELATION OF THE ATMOSPHERE	14
G.	WIND FIELD COMPLEXITY	17
III.	NETWORK MODELING OF THE PROBLEM	19
A.	CHAPTER OVERVIEW	19
B.	NETWORK MODEL	19
C.	NETWORK ARCHITECTURE.....	19
D.	ARC OPTIMIZATION.....	21
1.	Flight Speed Optimization in Zero Wind	21
2.	Effect of Wind	24
3.	Constraints on Airspeed	26
4.	Turning	28
5.	Climbing and Descending.....	31
6.	Effect of Flight Altitude.....	31
E.	ESTIMATION OF UAV PARAMETERS	33
IV.	NETWORK-SCALE OPTIMIZATION.....	35
A.	CHAPTER OVERVIEW	35
B.	MODEL I: DETERMINISTIC SHORTEST PATH.....	35
C.	MODEL II: STOCHASTIC-STATIC SHORTEST PATH.....	36
D.	MODEL III: STOCHASTIC-DYNAMIC SHORTEST PATH	40
E.	MODEL IV: CORRELATION-BASED STOCHASTIC-DYNAMIC SHORTEST PATH.....	44
F.	MODEL V: MAXIMUM DURATION STOCHASTIC-DYNAMIC SHORTEST PATH.....	46
G.	RESULTS	47
V.	CONCLUSIONS AND RECOMMENDATIONS.....	53
A.	CONCLUSIONS	53
B.	SUGGESTED WORK AHEAD.....	53

APPENDIX.....	55
LIST OF REFERENCES.....	57
INITIAL DISTRIBUTION LIST	61

LIST OF FIGURES

Figure 1.	Numerical results from the stochastic-dynamic model for 1000 simulations of 40 km round trips over Yucca Test Site, Nevada. Energy costs of the suggested paths are compared to the energy costs of straight-line paths for (a) 10 kg UAV and (b) 100 kg UAV.	xviii
Figure 2.	Numerical results from the maximum duration stochastic-dynamic model for 1000 simulations of 40 km round trips over Yucca Test Site, Nevada. Flight duration per unit energy was compared to the same ratio in the case of straight-line paths for a 100 kg UAV.	xix
Figure 3.	Plot of σ_v / \bar{V} as a function of \bar{V} for data collected at Marina Weather Station in 2002 with altitudes up to 1500 m.	8
Figure 4.	Plot of σ_θ as a function of \bar{V} for data collected at Marina Weather Station in 2002 with altitudes up to 1500 m.	9
Figure 5.	Decreasing vertical sigma levels, with respect to the ground altitude, in terrain-following coordinates, from top to bottom.	10
Figure 6.	Wind speed and direction fields for two forecasts, at 6 am and 9 am over a Yucca, Nevada test site, at altitude 1000 m.	12
Figure 7.	Histograms of (a) difference in wind directions and (b) difference in wind speeds, for three-hours-separated COAMPS forecasts at 6 am, and 9 am over Yucca, Nevada test site, at altitude 1000 m.	12
Figure 8.	Three components of the wind for weather forecasts produced by COAMPS for three different altitudes (left to right): 582 m, 1596 m and 2814 m, over Yucca, Nevada test site.	13
Figure 9.	Spatial correlation of the fluctuations in wind speed at increasing altitudes with respect to the wind speed at the lowest altitude available in five weather stations in California.	15
Figure 10.	(a) Example of the wind speed pattern throughout three days of measurements in Marina Weather station 10 m above ground level. (b) Temporal correlation of the wind speed. (c) Horizontal wind direction pattern for the same case. (d) Temporal correlation of the wind direction.	16
Figure 11.	Observed variations in the wind field as a function of altitude, up to 10 km, according to a 160 km x 160 km COAMPS forecast over Yucca, Nevada test site, for (a) wind speed and (b) wind direction.	17
Figure 12.	Example of outgoing arcs from five nodes in the network.	20
Figure 13.	Wind, air and ground velocities (\vec{V}_{wind} , \vec{V}_{Rel} and \vec{V}_{ij} respectively) and the corresponding angles β , α and γ_{ij} with respect to the horizon, on the plane created by \vec{V}_{wind} and \vec{V}_{ij} . Two cases are presented for clarification: (a) Tail wind (b) Head wind.	25
Figure 14.	Finding the lower bounds on the airspeed, $ \vec{V}_{Rel} $, using geometry, for two cases: (a) $ \beta - \gamma_{ij} \leq 90$ and (b) $ \beta - \gamma_{ij} \geq 90$	27

Figure 15.	A circular turn from arc (i, j) to arc (j, k) , with turn radius R , over θ degrees.	29
Figure 16.	Arc costs at altitudes up to 2000 m, for three different flight speeds, with the UAV parameters given in Table 2.	33
Figure 17.	(a) Arc costs [J] and (b) Suggested speed to fly as functions of wind speed and relative wind direction for the UAV parameters in Table 1.....	36
Figure 18.	Comparison of approximation (43) to the full integral in eq. (42), regarding the range of integration over wind speeds.	38
Figure 19.	(a) Expected arc costs [J] and (b) Expected speed to fly as functions of wind speed and relative wind direction for the UAV parameters in Table 1.....	39
Figure 20.	The expected cost-to-go convergence of the origin nodes in two sets of network realizations.	41
Figure 21.	Wind variation between adjacent nodes in terms of (a) wind speed and (b) wind direction.	42
Figure 22.	Illustration of a 100 km long round trip from top and side views of the suggested path to fly, using model III.....	48
Figure 23.	Averaged results from 1000 flight simulations, comparing the energy consumption of paths suggested by models I, II and III to the straight-line path with constant speed, as a function of the average wind speed along the direct $s-t$ path, for two UAV masses: (a) 10 kg and (b) 100 kg.	49
Figure 24.	Results from 1000 flight simulations, comparing the energy consumption of model III (Stochastic-Dynamic shortest path) to the straight line-path with constant speed, as a function of the average wind speed along the $s-t$ path, for two UAV masses: (a) 10 kg and (b) 100 kg.	50
Figure 25.	Results from 1000 flight simulations, comparing the increased flight duration per unit energy of model V (Stochastic-Dynamic Maximum Duration path) to the straight line-path with constant speed, as a function of the average wind speed along the $s-t$ path, for a 100 kg UAV.	51

LIST OF TABLES

Table 1.	Validation of COAMPS predicted wind speeds (From: [27]).	11
Table 2.	Representative values for a small UAV	32
Table 3.	Estimation errors of wind speed and direction in the form of standard deviations	43

THIS PAGE INTENTIONALLY LEFT BLANK

EXECUTIVE SUMMARY

The goal of this study is to provide a quantitative analysis of the potential energy savings for unmanned aerial vehicles (UAVs) through the use of wind currents. The idea is to implement a shortest-path network model, which provides the minimum-energy route between an initial point and a destination, using high-resolution three-dimensional weather forecasts and on-board dynamic estimations of the wind field. Energy savings can be directly translated to fuel or battery savings and may lead to longer flight distance and duration as well as improved operational flexibility.

High resolution or mesoscale weather forecasts are available from the Naval Research Laboratory's Coupled Ocean–Atmosphere Mesoscale Prediction System (COAMPS) model. This is a state-of-the-art numerical model applicable to any region of the world and provides 72-hours weather forecasts based on low resolution global weather data and the terrain features in the region of interest.

On-board estimations of wind fields are available on various UAVs that have global positioning systems and inertial navigation systems (GPS-INS module). For such UAVs, wind velocity estimates can be achieved by subtracting the UAV's ground velocity vector, given by the GPS, from its inertial velocity vector, given by the INS.

The following network-based models for finding minimum-energy paths were implemented:

1. A deterministic shortest-path model that assumes complete information about the wind field in the potential flight space. This model provides an upper bound for the possible energy savings.
2. A stochastic-static shortest-path model that uses a forecast of wind velocities and provides the path with the minimum expected energy cost. This corresponds to the case of a pre-flight routing plan without any dynamic updates.
3. A stochastic-dynamic shortest-path model that assumes a given weather forecast, as well as dynamic estimations of local wind fields through the on-board GPS-INS measurements.

The flight space is a three-dimensional box, which is divided into a grid of nodes, representing potential waypoints, with horizontal spacing of 1 km and vertical spacing of 100 m. Nodes are connected by arcs representing potential flight segments. Each node is connected only to its nearest neighbors in the general direction of flight including those along diagonals.

Network representation of energy consumption is achieved through the construction of an aerodynamic model of the UAV that provides the arc costs for the shortest path models. Since the network is discretized into relatively short flight segments represented by arcs, it is assumed that the wind velocity along each arc is constant, and that changes in the wind field lead to changes in the frame of reference of the UAV, but not to aerodynamic instabilities. Given a constant wind velocity, this study provides an analytical form for the energy cost of flight along an arc. This result is given as a function of the chosen airspeed, and of the following mechanical and aerodynamic parameters of the UAV:

- Mass
- Wingspan
- Parasite surface area
- Oswald's efficiency factor
- Engine's efficiency

Since the UAV's airspeed is a free parameter that can be changed through its flight, this study expands the arc cost formulation into a nonlinear optimization model that provides the best speed to fly on each arc to achieve minimum energy consumption on that arc. This nonlinear optimization model has the following constraints on the UAV's airspeed and air-velocity, for each arc in the network:

- The airspeed must be higher than the stall speed.
- The airspeed must be lower than the maximum value that can be achieved by the engine.
- The air velocity must be large enough to overcome the wind velocity and achieve a flight on the path defined by the given arc with a resulting ground speed that is higher than a certain minimum value.

The last constraint is found through the geometry of the problem by noticing that the air-velocity must lie on the same plane created by the ground and wind velocity vectors.

COAMPS forecasted wind fields with horizontal resolution of 1 km are transformed from terrain-following coordinates (sigma levels) into Cartesian coordinates and interpolated on the network, such that wind velocities are translated into arcs costs through the nonlinear optimization model. Vertical levels are linearly interpolated into 100 m grid spacing, in order to provide constant small climbing and descending angles in the range of +5.7 to -5.7 degrees.

Following the spatial interpolation of the forecasts, a temporal interpolation of a few different forecasts, at different points in time is performed. This is done in order to compensate for the fact that the UAV will reach different points in space at different times. This pre-processing interpolation is done under the assumption that the UAV will fly from origin to destination with a representative speed.

Wind speeds are modeled according to a two-parameter Weibull probability density function, and wind direction is modeled according to a normal probability density function. Both of these distribution functions are fitted in this work using observed quantities from the Marina weather station, California. This data includes measurements of wind speed and direction in altitudes up to 1500 m, throughout the year 2002. The vertical component of the wind is usually insignificant compared to the horizontal components. Hence, its distribution is ignored and, instead, the vertical forecasted wind speed is taken as constant.

Model I: Deterministic Shortest-path

The deterministic shortest-path model uses statistical knowledge about the wind and a wind forecast to create a realistic wind field for the area of interest. Dijkstra's algorithm is then used to find the path with the minimum energy cost from origin to destination. This corresponds to the ideal case, where complete information about the arc costs on the network is given. Results from this model serve as an upper bound on the optimal energy savings for the other models.

Model II: Stochastic-static Shortest-path

The stochastic-static shortest-path model uses the statistical behavior of the wind to calculate the expected (average) arc costs on the network and use these to find the shortest path with Dijkstra's algorithm. This model represents the case of no flight plan updates during the flight. Results from this model serve as a lower bound on the energy savings for the stochastic-dynamic model. The expected arc costs are calculated through the averaging of many realizations, or by the use of a pre-constructed table of energy costs, for every wind velocity (one value for every combination of speed and direction).

Model III: Stochastic-dynamic Shortest-path

The stochastic-dynamic shortest-path model uses an approximate dynamic programming algorithm that provides the expected cost-to-go from each node to the destination node. This model dynamically re-optimizes the UAV's route based on dynamically collected information about the local wind field. The calculation of the expected cost-to-go from each node is carried out prior to actual flight and only uses the probability distributions of the arc costs. Specifically, the expected cost-to-go is calculated through a converging algorithm that starts with an initial guess for the expected cost-to-go. Each iteration updates the expected cost-to-go at a node using a randomly generated realization of the on-board wind velocity measurement corresponding to the outgoing arcs of the current node as well optimization of the possible moves from this node. Given the expected cost-to-go, the required calculations during flight is trivial: At each node in the network, the UAV measures the wind and determines the optimal arc to proceed on using that measurement and the expected cost-to-go. This model has a recursive nature. It assumes that the best decision will be made at every point in the future, based on the information available at that point.

Errors in the dynamic estimation of the wind velocity are simulated through the use of available data in the literature regarding the accuracy of GPS-INS systems. A "spatial fluctuation error" is also taken into account to represent the different wind velocities in different points along the arcs. This is done by calculating the variation in wind velocities for the collection of all adjacent node pairs in the forecast.

Model IV: Correlated-based Stochastic-dynamic Shortest-path

This model uses a correlation-based stochastic-dynamic shortest-path algorithm, which utilizes the spatial correlation structure of the wind to improve the accuracy in the estimation of the distribution of wind velocities. This model assumes a spatially-autocorrelated joint distribution for the wind velocities, instead of independent marginal distributions as was assumed in the previous models. This model was not implemented in a simulation, as data on the spatial correlation structure of wind was not available at the time of the study. Experimental data may be achieved by simultaneous measurements of wind velocities in different altitudes over a set of nearby locations. The main drawback of this proposed model is, however, its expected heavy computational requirements and long processing time.

Model V: Stochastic-dynamic Maximum Duration Path

In addition to the minimum-energy models, a heuristic maximum-duration model is constructed based on the stochastic-dynamic model. This model also assumes a back-and-forth flight path between two points and instead of minimizing energy per distance, it minimizes the energy per unit time, or maximizes the duration of flight per unit of energy.

The first three models and the fifth model are implemented in MATLAB, using COAMPS weather forecasts over a 160 km-by-160 km region at Yucca Air Force Test Site, Nevada. 1000 north-south and east-west paths of 40 km round trips (approximately 20 km ingress plus 20 km egress) are simulated through a Monte Carlo numerical simulation. Origins and destinations points are chosen randomly within the constraint that they lie no less than 100 meters above the highest terrain features in the area of flight. Each of the models produces a suggested flight path and an associated energy cost, which is compared to the energy cost of a straight line flight path with a constant speed.

As expected, the deterministic model provides an upper bound on the amount of energy savings for the other models. The stochastic-dynamic model produces results that are significantly better than the stochastic-static model. The latter model produces energy savings of no more than 10%. Results for the stochastic-dynamic model are shown in Figures 1a and 1b, for representative 10 kg and 100 kg UAVs.

For a 100 kg UAV, the stochastic-dynamic model produces an average reduction of 15% in the energy consumption, compared to the straight-line paths, and an average reduction of 30% under windy conditions with average wind speeds larger than 15 m/s. The model provides significant improvements in head-wind scenarios, in which the optimized flight paths avoided stronger wind currents. Conversely, the model does not provide significant improvements in tail-wind scenarios, where the optimized flight paths are similar to straight-line paths.

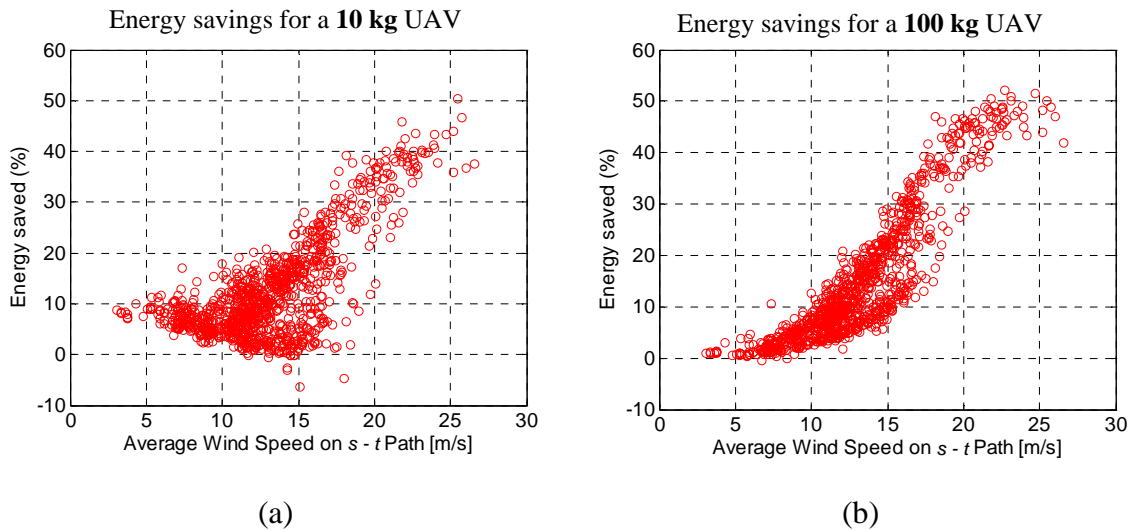


Figure 1. Numerical results from the stochastic-dynamic model for 1000 simulations of 40 km round trips over Yucca Test Site, Nevada. Energy costs of the suggested paths are compared to the energy costs of straight-line paths for (a) 10 kg UAV and (b) 100 kg UAV.

The maximum-duration model is implemented using the same data and 1000 randomly generated scenarios, but now without the horizontal degrees of freedom. That is, the UAV cannot deviate from a straight line, which corresponds to a border-patrol

scenario. Results for a 100 kg UAV are shown in Figure 2. On average, an increase of 32.2% in the flight duration is achieved, compared to a straight-line flight with a constant speed.

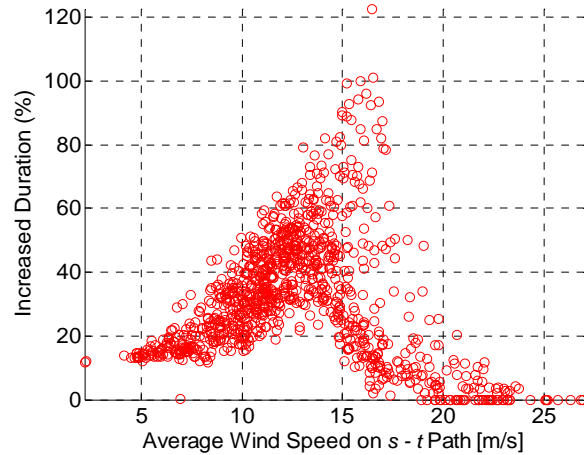


Figure 2. Numerical results from the maximum duration stochastic-dynamic model for 1000 simulations of 40 km round trips over Yucca Test Site, Nevada. Flight duration per unit energy was compared to the same ratio in the case of straight-line paths for a 100 kg UAV.

In conclusion, numerical simulations has shown that accounting for wind currents during flight path planning may result in a significant reduction of energy consumption for various UAVs without any additional hardware. Avoidance of strong head winds is shown to have the largest impact on energy consumption.

THIS PAGE INTENTIONALLY LEFT BLANK

ACKNOWLEDGMENTS

The author would like to acknowledge the following contributors to the work:

Professor Johannes O. Royset, for his thorough guidance on algorithms, networks and statistical methods and for constantly making sure that the work is on the right path,¹

Professor Kevin Jones, for his invaluable advices on aerodynamics and mechanics of UAVs,

Dr. Jason Nachamkin, for his comprehensive instruction on the interpretation and analysis of COAMPS weather forecasts,

Professor Richard (Dick) Lind, for providing critical data for this thesis from his measurements in the Marina weather station, California,

Maj. Jim Wong and Ms. Oh Pei Tze for their continuous help, encouragement and good ideas,

And the Naval Postgraduate School and Naval Research Laboratory staff who shared their knowledge and insights with much kindness.

¹ Though not necessarily on the minimum-energy path.

THIS PAGE INTENTIONALLY LEFT BLANK

I. INTRODUCTION

A. MOTIVATION

Unmanned aerial vehicles (UAVs) are expected to become an important force multiplier on the future battlefield. They will have a profound impact in the areas of Intelligence, Surveillance, and Reconnaissance (ISR), Suppression of enemy defenses (SEAD), Electronic Warfare (EW), and attack/strike operations [1],[2]. The amount of time a UAV can stay in the air and the maximum distance it can reach are critical factors for all these missions. Atmospheric drag forces and the UAV's energy resources (gasoline or battery) restrict the flight range of the UAVs. As UAVs are made increasingly smaller, this restriction becomes more and more prominent due to the smaller weight allocated to battery and fuel compartments. The energy consumption of a UAV can sometimes be improved through changing its structural design or flight velocity [3], but also through a better use of available air currents and gusts. This thesis will analyze, by means of minimum energy path models, the possibility of using the wind as a way to reduce energy consumption.

B. THESIS OBJECTIVE AND SCOPE

The objective of this work is to provide a quantitative analysis of the potential energy savings for UAVs through the use of wind currents. The idea is to implement shortest-path network models, which provide the minimum-energy or maximum-flight-duration route between an initial point and a destination, using high-resolution three-dimensional weather forecasts and on-board dynamic estimations of the wind field. These models are based on the stochastic behavior of the wind and utilize mesoscale wind forecasts and on dynamic updates of the wind velocity by means of onboard measurements throughout the UAV's flight. A significant portion of the work focuses on the conversion of aerodynamic and physical characteristics of a flight in a wind field into a network model formulation.

The proposed models are capable of handling complex wind structures. At low altitudes - up to 2 km - there are usually more frequent changes in the wind direction. Conversely, at higher altitudes,² wind currents are relatively constant and the optimal flight paths are usually easy to predict. Hence, this thesis targets UAV missions at low altitudes where route optimization models may be most beneficial. Since weather forecasts are currently available at the horizontal resolution of 1 km, this study focuses on mission with flight lengths significantly greater than 1 km.

C. POTENTIAL BENEFITS OF THE STUDY

Energy conservation can be directly translated to fuel and battery savings and may lead to longer flight distance and duration, and a higher flexibility in real-time decisions regarding a UAV mission. Implementation of the proposed shortest-path models requires only software modifications in the control station of the UAV. No hardware changes are typically needed as most UAVs already have the necessary instruments such as global positioning system (GPS) and inertial navigation system (INS) for measuring wind.

D. RELATED WORK

There are several studies on optimal routing of UAVs with respect to energy resources, target acquisition and obstacles avoidance. These studies have considered both deterministic and stochastic situations and have derived methods based on, for example, potential fields [4], graph search methods [5] and evolutionary algorithms [6],[7],[8].

Paul McCready published his theory in the early 1950s on rules for efficient gliding, and specifically, guidelines for optimal flight between thermals (“MacCready Speed,” see [9]). Since then, these guidelines have served as a significant help to pilots’ intuition. A large amount of work has since been done on energy efficient speeds and trajectories for gliders and utilization of thermals for “soaring.” These studies include the use of optimal control, parameter optimization and the variational formulation [9]-[13], to achieve improved paths (higher or faster flight) using local observations of vertical currents. These models can be helpful in UAV missions either through reduction of

² See Figure 11, p. 17.

energy consumption by leveraging the wind, or by reducing the engine's noise for the purpose of concealment [14]. Due to the unpredictable behavior of thermals, the models in these studies provide only locally-optimal paths under initial constraints, and do not make use of large scale wind currents forecasts.

Large-scale optimization of flight duration and fuel consumption is frequently used in commercial aircrafts. This is done through the use of jet streams and real-time weather forecasts of high-altitude wind currents [15]. The stochastic and dynamic behavior of weather obstacles, such as storms is also studied [16]. In the world of UAVs, evolutionary algorithms are used to find an adaptive optimized path, using large-scale wind fields, e.g., for a Trans-Pacific Crossing [8], or adaptive obstacle avoidance [6].

None of the above studies utilize low-altitude, high-resolution weather forecasts for minimum-energy or maximum-duration paths. This thesis will use such forecasts and formulate network models that provide optimal paths for the case of low-altitude UAV flights.

E. THESIS ORGANIZATION

Chapter II discusses the nature of wind, presents an analysis of weather data from the Marina weather station, and describes COAMPS mesoscale weather forecast model of the Naval Research Laboratory (NRL). Chapter III discusses the construction of a network model and an aerodynamic model for the energy cost of flight along an arc in the network. Chapter IV describes the five network models for minimum-energy paths: a deterministic model that assumes perfect knowledge, a stochastic-static model for a pre-flight plan, a stochastic-dynamic model that takes into account dynamic measurements, a correlation-based stochastic-dynamic model that considers the correlation structure of the atmosphere and a maximum-duration model for the maximization of the flight time. Chapter V discusses the implementation of the models in a simulation of flights above a Nevada test site, and presents numerical results. Chapter VI concludes the work.

THIS PAGE INTENTIONALLY LEFT BLANK

II. WIND AND FORECASTS

A. CHAPTER OVERVIEW

Our study is motivated by the potential of energy savings for unmanned aerial vehicles (UAVs) through the use of wind currents. In this chapter, the statistical characteristics of wind are discussed, followed by analysis of weather data collected in the Marina weather station and a description of COAMPS weather forecasts. The general way in which wind data and forecasts will be implemented in our network models is also discussed. This includes the temporal and spatial correlation structure of the wind velocity, which serves as a basis for a correlation-based shortest path model.

B. WIND BEHAVIOR

Wind – the flow of air in the atmosphere – is caused by pressure gradients. On the global scale, the major driving factors for wind are the sun’s uneven heating of the earth and the Coriolis force, which is created by the rotation of the earth. In mesoscale wind, which is on the scale of hundreds of meters up to tens of kilometers, the main driving effects are differential heating³ and terrain features. Micro-scale winds exist on the scale of tens to hundreds of meters (e.g., thermals), and are essentially unpredictable.

On small scales, wind speed and wind direction can both be seen as random variables. The observed quantities will be distributed around some mean value. Wind speeds are frequently modeled according to a two-parameter Weibull probability density function [17]-[20]. This thesis assumes that the wind direction has a normal probability density function with the forecasted direction as its mean. Both of these distribution functions are fitted in this work using observed quantities.

³ For example, in the case of a sea breeze, the source for differential heating is the land’s faster heating during the day and cooling during the night compared to the sea, which leads to a lower pressure above the sea during the days and a higher pressure throughout the evenings and nights.

The Weibull distribution has the following probability density function:

$$(1) \quad f(V) = \frac{k}{c} \left(\frac{V}{c} \right)^{k-1} \exp \left[- \left(\frac{V}{c} \right)^k \right],$$

$$V \geq 0, k > 0, c > 0,$$

and the cumulative probability distribution function:

$$(2) \quad F(V) = \int_{-\infty}^V f(V) dV = 1 - \exp \left[- \left(\frac{V}{c} \right)^k \right],$$

where V is the wind speed and k and c are the two parameters of the distribution. The mean and variance of the Weibull distribution are given by:

$$(3) \quad E(V) = c \Gamma \left(1 + \frac{1}{\beta} \right),$$

and:

$$(4) \quad Var(V) = c^2 \left[\Gamma \left(1 + \frac{2}{\beta} \right) - \left[\Gamma \left(1 + \frac{1}{\beta} \right) \right]^2 \right],$$

where Γ is the gamma function in the positive domain:

$$(5) \quad \Gamma(z) = \int_0^{\infty} t^{z-1} \exp(-t) dt, \quad z > 0.$$

There are several methods of determining the parameters c and k . One of them [18] uses the mean and standard deviation of the wind speed to find c and k as follows:

$$(6) \quad k = \left(\frac{\sigma_V}{\bar{V}} \right)^{-1.086},$$

and:

$$(7) \quad c = \frac{\bar{V}}{\Gamma \left(1 + \frac{1}{k} \right)}.$$

Here, \bar{V} is the mean wind speed, and σ_v is the standard deviation of the wind speed. This method is used here together with wind observations and the forecasted wind speed values, as detailed in section II.C.

A random variable V that follows a Weibull distribution can be created using a uniformly distributed random variable and the Inverse Method for the cumulative distribution function in eq. (2). In this work, uniformly distributed random variables $\chi \sim Un(0,1)$ are generated using MATLAB's random variable generator and the random wind speed, V , is calculated through:

$$(8) \quad V = F^{-1}(\chi) = \left[-\ln(1-\chi) \right]^{1/k} c.$$

The normal distribution of the wind direction, θ , has the following parameters:

$$(9) \quad g(\theta) = \frac{1}{2\pi\sigma_\theta} \exp\left(-\frac{(\theta - \theta_0)^2}{2\sigma_\theta^2}\right),$$

where σ_θ is the standard deviation and θ_0 is the average wind direction. The random variable θ is created using MATLAB's generator for normally distributed random variables. It is assumed that the forecasted wind direction is an unbiased prediction and equals its average value θ_0 . σ_θ is calculated using observation data and forecasted wind speed values as detailed in the following section.

C. WIND DATA

In the proposed models, the parameters of the two distribution functions for the speed and direction are computed from data from the Marina weather station, California, for the year 2002, collected by the Department of Meteorology of the Naval Postgraduate School (NPS) [21]. This data was collected continuously at 40 different altitudes up to 1500 m and averaged over periods of 30 minutes using NPS 915 MHZ wind profiler, a Doppler based three beams radar for measurements of the three components of the wind [22],[23].

Analysis of the data collected reveals a consistent relation between σ_V and \bar{V} , and also a consistent relation between σ_θ and \bar{V} . These relations are used as a basis for our simulations. The following approximated relations are found through fitting of the observed relations by a polynomial of the third degree for \bar{V} :

$$(10) \quad \frac{\sigma_V}{\bar{V}} \approx \begin{cases} -5.6 \cdot 10^{-4} \bar{V}^3 + 1.75 \cdot 10^{-2} \bar{V}^2 - 0.178 \bar{V} + 0.701, & 0 \leq \bar{V} \leq 15 \\ 0.1, & \bar{V} > 15 \end{cases},$$

$$(11) \quad \sigma_\theta \approx \begin{cases} -5 \cdot 10^{-2} \bar{V}^3 + 1.63 \bar{V}^2 - 17.63 \bar{V} + 69.41, & 0 \leq \bar{V} \leq 15 \\ 6, & \bar{V} > 15 \end{cases}.$$

Here, σ_V and \bar{V} are given in m/s, and σ_θ is given in degrees. These approximations for the statistical measures of the wind are found by dividing the year of observations into two-hour periods in order to achieve results for temporally local fluctuations while allowing enough observations (of 30 minutes intervals) per calculation.

Comparison of these approximations to the observed data is shown in Figures 3 and 4. Less data is available for higher wind speeds (>15 m/s). Hence, a constant fitted value is used to avoid over-fitting of the fluctuations.

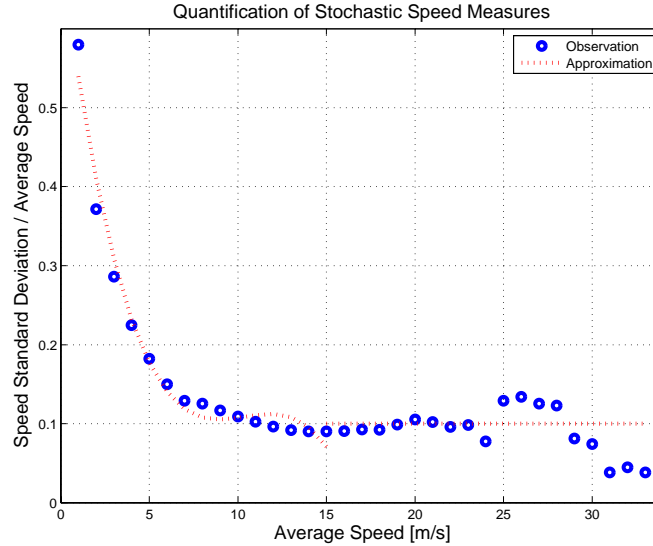


Figure 3. Plot of σ_V / \bar{V} as a function of \bar{V} for data collected at Marina Weather Station in 2002 with altitudes up to 1500 m.

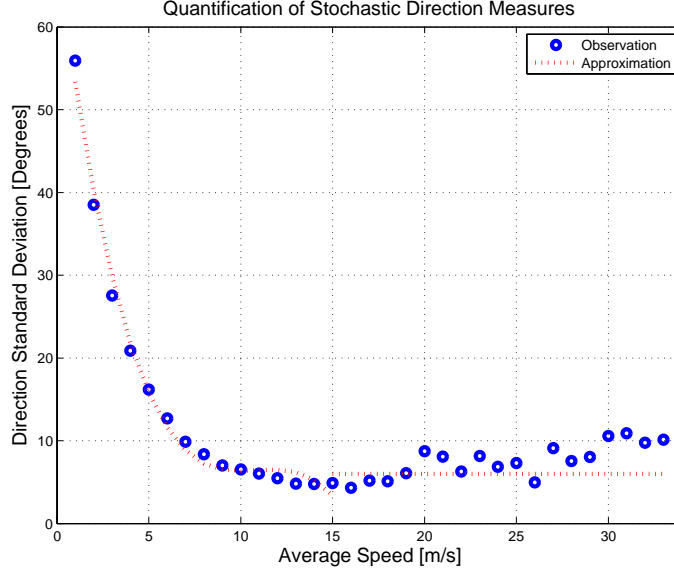


Figure 4. Plot of σ_θ as a function of \bar{V} for data collected at Marina Weather Station in 2002 with altitudes up to 1500 m.

Eqs. (10) and (11) are implemented in this study using \bar{V} as the forecasted wind speed, and θ_0 as the forecasted wind direction, such that the standard deviations σ_v and σ_θ are calculated from \bar{V} only.

D. MESOSCALE WEATHER FORECASTS

Mesoscale weather forecasts are characterized by horizontal grid resolutions on the scale of ten kilometer down to hundreds of meters. These forecasts are created by modeling the atmosphere of a certain region as a three-dimensional array of cells, where each cell is characterized by its physical attributes, such as air temperature, pressure, density, humidity etc. In these forecast models, application of numerical models for the governing physical equations of the atmosphere, given initial and boundary conditions, leads to a set of forecasts for a collection of points in time.

COAMPS–Coupled Ocean–Atmosphere Mesoscale Prediction System—is a state-of-the-art weather forecast model for high resolution short-term (up to 72 hours) predictions built by Naval Research Laboratory (NRL) [26]. This model provides various

weather characteristics in time intervals of down to one hour and with horizontal spatial resolution of down to 1 km. Vertical levels are given in the form of sigma levels, or terrain following coordinate system [26]. In order to convert the forecasts into Cartesian coordinates, the definition of the terrain-following coordinates is used:

$$(12) \quad \sigma = s \frac{z - z_G}{s - z_G},$$

or:

$$(13) \quad z = z_G + \sigma \left(1 - \frac{z_G}{s} \right),$$

where σ is the sigma coordinate, z_G is the ground altitude, s is the maximal altitude in the model and z is the desired Cartesian altitude. COAMPS uses 60 sigma levels, for altitudes up to 30 km, as shown in Figure 5.

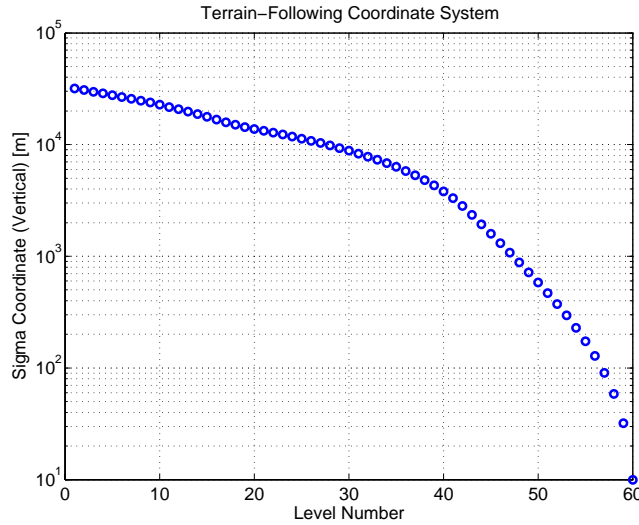


Figure 5. Decreasing vertical sigma levels, with respect to the ground altitude, in terrain-following coordinates, from top to bottom.

Various tests were conducted to assess the accuracy of COAMPS forecasts, see [23],[24],[27]. Measured values of wind speeds were recently compared to the forecasted values by Nachamkin et al., [27]. Measurements were made in 10 m altitude, and produced the results of Table 1 for low wind speeds (up to 4 m/s), with a 1 km grid

spacing model. These measurements show that the biases in the forecasted wind measures are significantly smaller than the standard deviations and hence, this thesis assumes that the wind forecasts are unbiased estimators for the distributions of wind speeds and directions.

Table 1. Validation of COAMPS predicted wind speeds (From: [27]).

Speed bias	0.53 m/s
Speed standard deviation	1.75 m/s
Direction bias	1.28 degrees
Direction standard deviation	75.2 degrees

E. USING FORECASTED WIND FIELDS

This study uses only the three components of the wind velocity in every point in the grid, and does not make use of the various other physical parameters provided by the forecasts [26]. Let us denote these components by: $V_u(x, y, z, t)$, $V_v(x, y, z, t)$ and $V_w(x, y, z, t)$, where x , y and z are the spatial coordinates in the region of interest, t is the point in time for which the forecast refers to and u , v and w denote each of the Cartesian wind components in the x , y and z directions, respectively.

After performing a spatial transformation of the terrain-following coordinates into a Cartesian grid, through eq. (13), wind components are interpolated into a constant vertical spacing, using a linear approximation. This is done in order to assure low angles of climb and descent when implementing a simulated flight and avoid non-linearity in the drag-to-lift ratio [29]. Since the differences between forecast times are small (down to one hour), linear approximation for the change in the three components of the wind velocity is used in the interpolations. Differences in the forecasted wind speed, $|\vec{V}_{wind}|$ and wind direction, θ , within 3 hours, are presented as contour plots over a 50 km by 50 km area in Figures 6 and 7. Angles are taken with respect to the north, counterclockwise. It is noticed that the wind field experiences a general acceleration and a clockwise shift in

the later forecast, compared to the earlier one. The three components of the wind are shown for different altitudes in Figure 8. Generally, the vertical component is negligible compared to the horizontal ones.

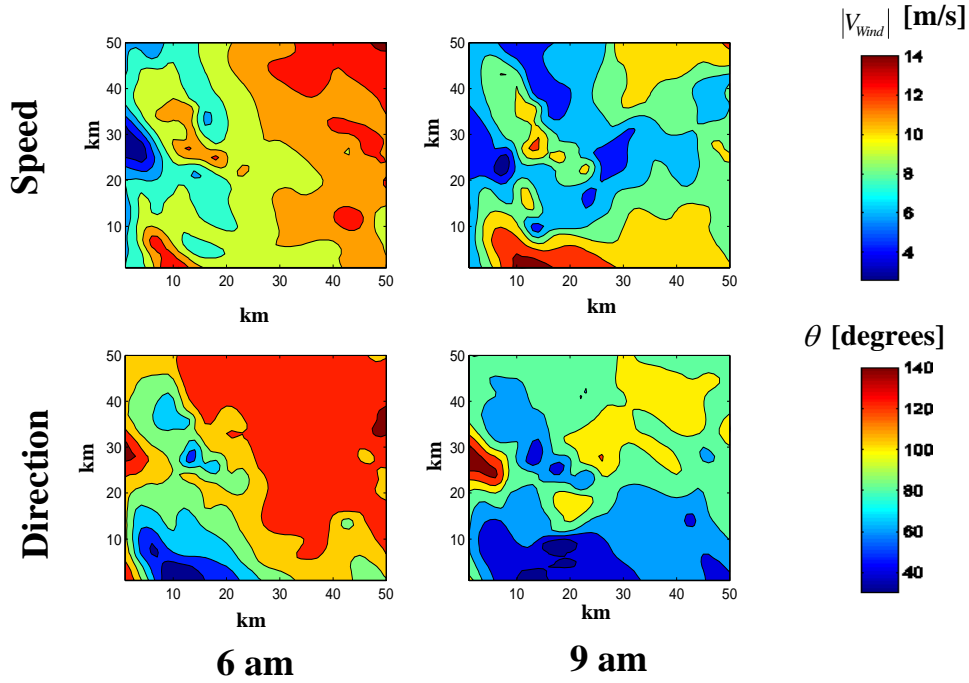


Figure 6. Wind speed and direction fields for two forecasts, at 6 am and 9 am over a Yucca, Nevada test site, at altitude 1000 m.

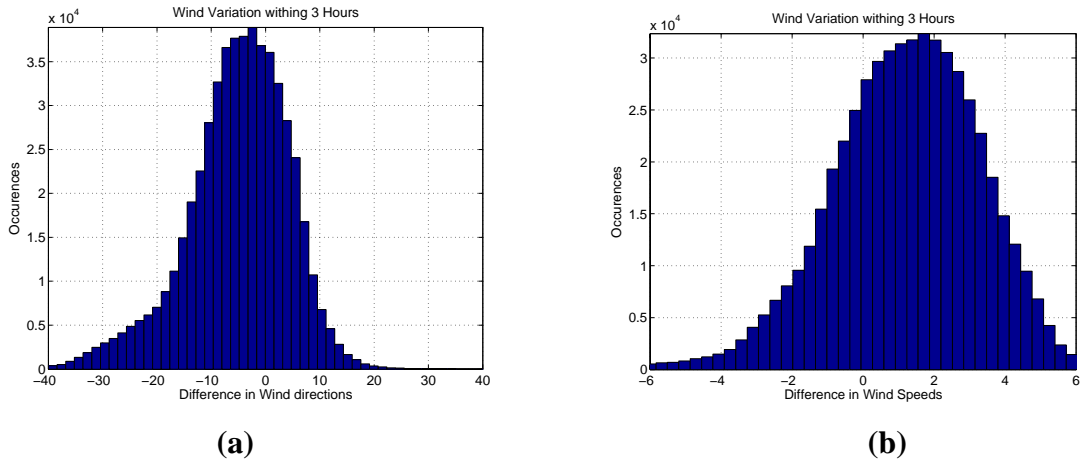


Figure 7. Histograms of (a) difference in wind directions and (b) difference in wind speeds, for three-hours-separated COAMPS forecasts at 6 am, and 9 am over Yucca, Nevada test site, at altitude 1000 m.

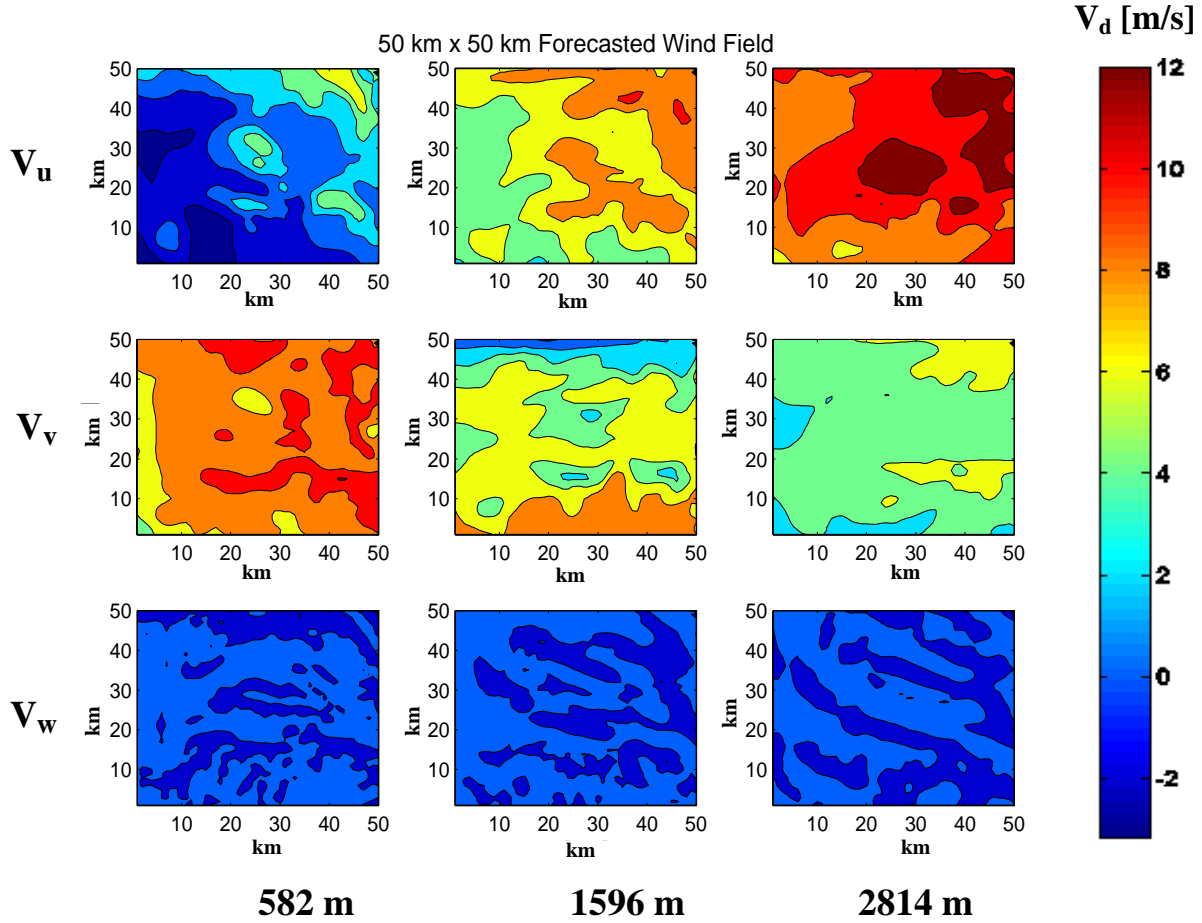


Figure 8. Three components of the wind for weather forecasts produced by COAMPS for three different altitudes (left to right): 582 m, 1596 m and 2814 m, over Yucca, Nevada test site.

Since this study uses a stationary probability model of the wind it will not matter when the UAV arrives at an arc—the arc will always have the same wind velocity distribution. Therefore, a temporal interpolation of a few different forecasts, at different points in time follows the spatial interpolation of the forecasts. This is done in order to compensate for the fact that the UAV reaches different points in space at different times. This pre-processing interpolation is done under the assumption that the UAV will fly from origin to destination with a representative speed.

Temporal interpolation of forecasts is done through the following equation:

$$(14) \quad V_d^*(\vec{r}) \equiv V_d^*(x, y, z) = V_d^1(x, y, z, t_1) + \alpha(V_d^2(x, y, z, t_2) - V_d^1(x, y, z, t_1)),$$

where $\vec{r} = (x, y, z)$ is a coordinate of V_d^* , the interpolated grid component $d \in \{u, v, w\}$, V_d^1 is the forecast at time t_1 , V_d^2 is the forecast at time t_2 and α is the interpolation factor, calculated by:

$$(15) \quad \alpha(x, y, z) = \frac{\left(\frac{|\vec{r} - \vec{r}_0|}{V_0} \right)}{t_2 - t_1} = \frac{\sqrt{(x - x_0)^2 + (y - y_0)^2 + (z - z_0)^2}}{V_0(t_2 - t_1)},$$

where $\vec{r}_0 = (x_0, y_0, z_0)$ is the coordinate of the origin and V_0 is an estimation for the UAV's speed along its flight path.

It is noticed that for an interpolation at a point in time between two forecasts to be possible, and not become an extrapolation, $\alpha(x, y, z)$ must obey the following equation:

$$(16) \quad 0 \leq \alpha(x, y, z) \leq 1.$$

Projection of the grid on the Earth's coordinates is unnecessary in our models, since the scales of interest are of dozens of kilometers, in which the curvature of the earth is not significant.

F. TEMPORAL AND SPATIAL CORRELATION OF THE ATMOSPHERE

Temporal and spatial correlation characteristics of the atmosphere may be incorporated in a minimum-energy model for better predictability of the wind behavior and improved energy conservation. This section discusses the correlation structure of the wind, in the context of shortest-path models.

Since forecasted wind fields are assumed to have the average values of the three components of the wind distribution, this study is interested in the structural correlation of the *fluctuation* of the wind around its average values. Correlation may be calculated for any two points in time and space. Models for the complete correlation structure of the

atmosphere, in general, or experimental data for specific regions was not available at the time of the study. However, analysis of the spatial correlation at different altitudes and the temporal correlation at one location reveals partially, as seen in Figures 9 and 10, the complete space and time correlation structure of the wind fluctuations.

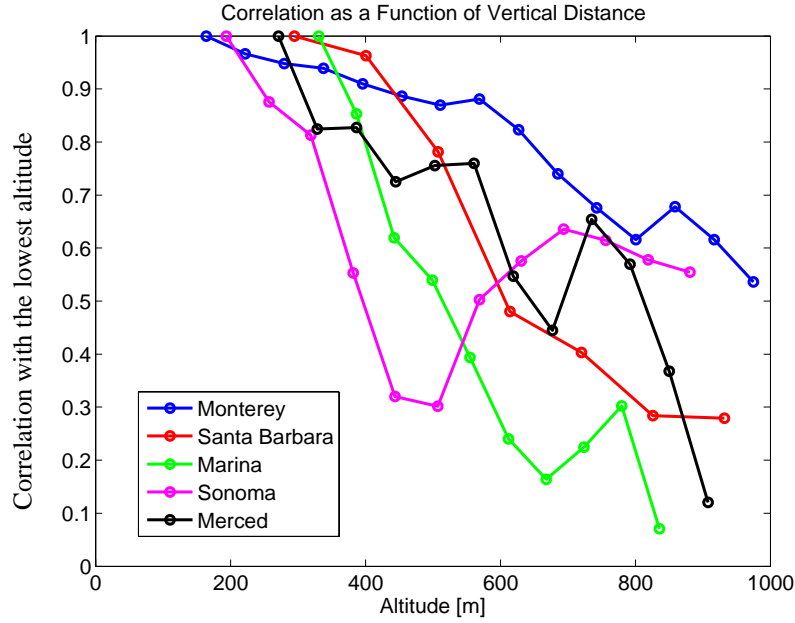


Figure 9. Spatial correlation of the fluctuations in wind speed at increasing altitudes with respect to the wind speed at the lowest altitude available in five weather stations in California.

It is observed in Figure 9 that the correlation in the wind speed remains above 0.8 for spatial separations of up to 300 m. Figure 10 reveals that also the temporal correlation of the wind speed and direction remains quite high for the short term. In these experiments, a correlation higher than 0.8 is observed for up to 70 minutes regarding the wind speed, and up to 25 minutes regarding the wind direction. High correlation values may be used for better estimation of the wind at different locations and times given local measurements, and therefore provide better results for the shortest path models.

Figure 10 presents measurements of the wind speeds and directions at two-minute intervals. The temporal correlation structure is calculated according to these periodic measurements recorded throughout 2002. High correlation is seen at intervals of exactly 24 hours due to the consistent weather cycle near the ocean (e.g., sea breezes in the evenings.)

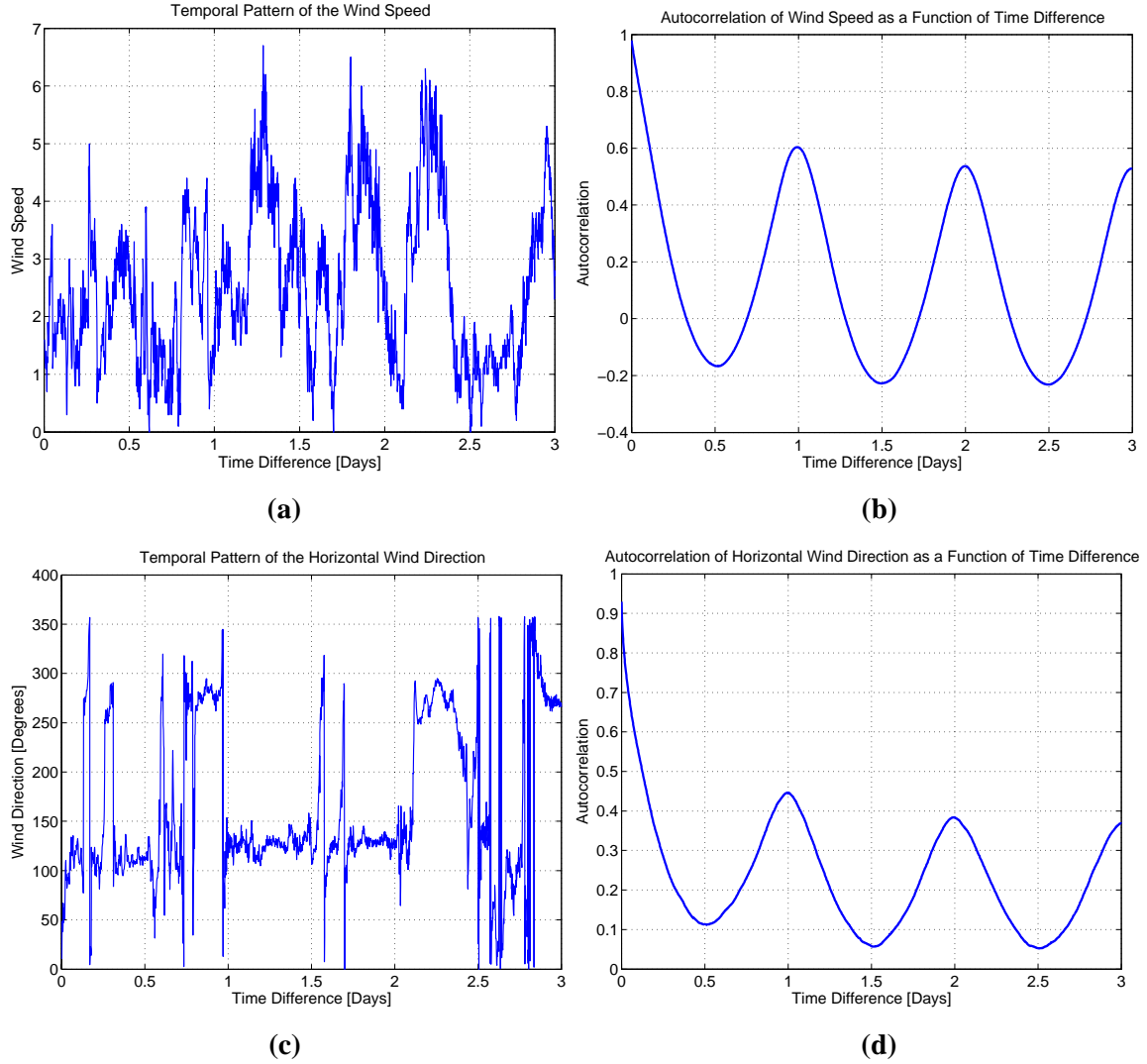


Figure 10. (a) Example of the wind speed pattern throughout three days of measurements in Marina Weather station 10 m above ground level. (b) Temporal correlation of the wind speed. (c) Horizontal wind direction pattern for the same case. (d) Temporal correlation of the wind direction.

G. WIND FIELD COMPLEXITY

The shortest-path models were tested for flights at different altitudes. It was observed that when the wind field is approximately constant, then the resulting minimum-energy paths became similar to the straight line paths. When the simulated flight altitude increases, a similar result is noticed. Therefore, the effect of altitude on the complexity of the wind field, or the amount of variation in the wind speed and direction as a function of the altitude, is analyzed in Figure 11. Generally, the standard deviation of the wind directions at the same altitude is low for altitudes of 2 km and above. Variation in the speed reaches its highest value just below 2 km. Thus, it is assumed that the models presented in this work will provide a significant improvement mostly for low-altitude flights below 2 km.

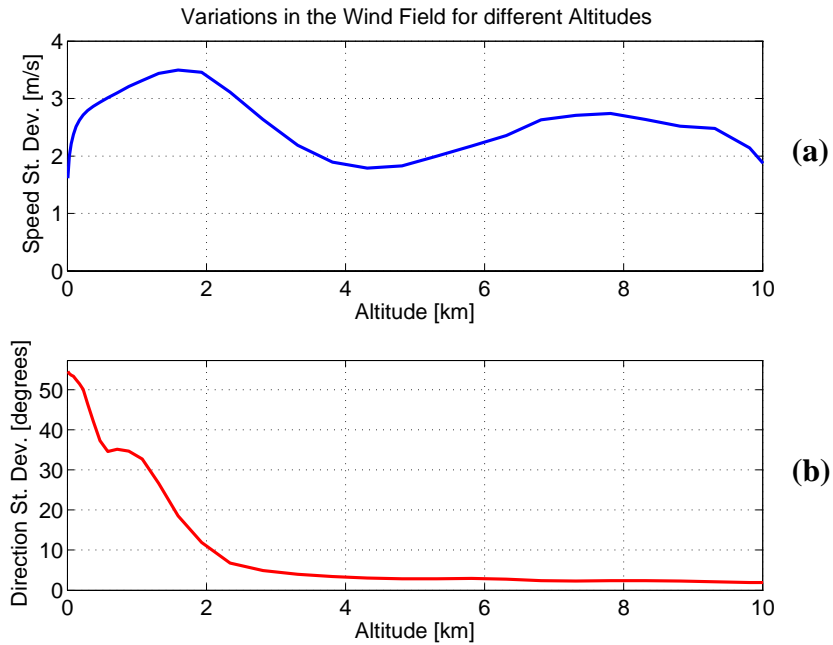


Figure 11. Observed variations in the wind field as a function of altitude, up to 10 km, according to a 160 km x 160 km COAMPS forecast over Yucca, Nevada test site, for (a) wind speed and (b) wind direction.

THIS PAGE INTENTIONALLY LEFT BLANK

III. NETWORK MODELING OF THE PROBLEM

A. CHAPTER OVERVIEW

In this chapter, a network model of the airspace is constructed, as well as an aerodynamic model for the energy cost of a flight on each arc in the network.

B. NETWORK MODEL

The problem of finding a minimum-energy path between an initial UAV location and a destination can be solved using network-based shortest-path models and algorithms. The airspace is divided into a grid of nodes, which represent potential waypoints. Adjacent nodes are connected by arcs, which represent potential flight paths between neighboring waypoints. Let us define a network (N, E) , where N is the set of nodes and E is the set of arcs. Arcs are denoted by $(i, j) \in E$, where $i, j \in N$ are adjacent nodes.

C. NETWORK ARCHITECTURE

The spatial orientation of the network is defined such that the grid is aligned with the direction of the straight-line between the initial UAV location and its destination. The network can then be built around the straight-line path, and the minimum-energy path can be directly compared to the straight-line path.

In order to contain the network's size and subsequently the runtime of the algorithms, the flight is restricted to always have a "forward" component. In other words, the only outgoing arcs from each node will be those that are directed towards the neighboring nodes in the forward plane, as depicted in Figure 12. Every node that is not on the boundary of the network has nine outgoing arcs in the general direction of flight.

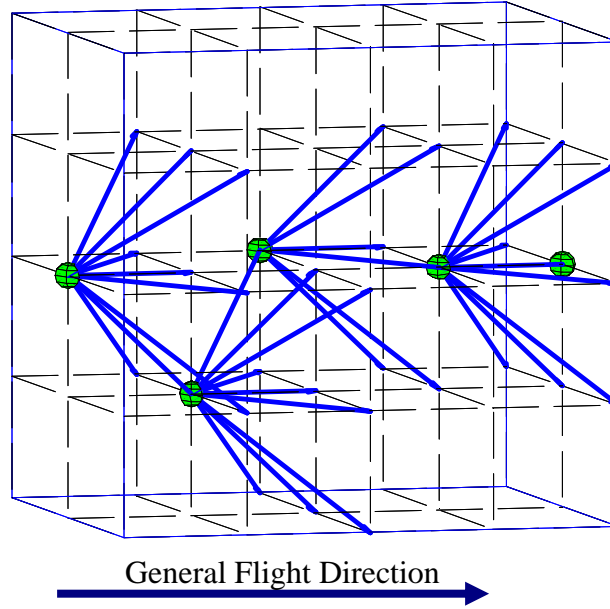


Figure 12. Example of outgoing arcs from five nodes in the network.

The horizontal spacing is 1 km, whereas the vertical spacing is 100 m. This leads to four potential arc lengths: 1 km, 1.005 km, 1.41 km, 1.42 km and produces small angles of climb and descent. As mentioned in Chapter II, these small angles help in avoiding non-linearity in the drag-to-lift ratio [29] and maintains the validity of the aerodynamic expressions.

Nodes and arcs are represented in a forward-reverse star data structures to facilitate quick access of information by the different algorithms [30]. In order to avoid individual consideration of every type of nodes (i.e., corners/edges/inner nodes – 27 types in total for a three dimensional rectangular network) during the initialization of the networks, none of the boundary nodes contain any outgoing arcs to the rest of the network. This ensures that the inner nodes will still have exactly nine outgoing arcs to the forward layer, while reducing extra checks for those nodes that have between one and eight outgoing arcs to the forward layer. If this individual “care” was given for every node type in the network throughout the execution of the shortest-path algorithms (e.g., Dijkstra’s [30]), it would result, for example, in a computational cost of $O(n^3)$ for a

cubic network, where n is the number of nodes in one axis of the cube. The price is an extra $O(n^2)$ for every execution of the shortest-path algorithm, since all boundary nodes are practically meaningless to the solution, but are still taken into account since arcs are directed towards them, in general. This turns out to be useful particularly in cases where statistics are made using many different path samples of a certain area, and the algorithm is executed once for every initialization of the network, so the extra $O(n^3)$ operations are essentially replaced by extra $O(n^2)$ operations.

D. ARC OPTIMIZATION

Before discussing the network-scale shortest-path optimization, this study investigates the optimal way to cross an arbitrary arc in the network, under the UAV's two degrees of freedom: flight speed and direction. This optimization is referred to as "arc optimization."

1. Flight Speed Optimization in Zero Wind

In [3], Carson shows that the most fuel-efficient flight speed (later known as "Carson's speed"), in the case of zero wind, can be expressed as a function of the aircraft's aerodynamic characteristics. This study will follow Carson's framework [3], and assume a drag-to-lift ratio that can be approximated as:

$$(17) \quad \frac{D}{L} = AV^2 + B/V^2,$$

where V is the flight speed and, A and B are given by:

$$(18) \quad A = \frac{\rho(h)f}{2W},$$

$$(19) \quad B = \frac{2W}{\rho(h)b^2\pi e}.$$

Here, $W = mg$ is the aircraft's weight, given by multiplication of its mass by the gravitational acceleration, $\rho(h)$ is the air density at altitude h , b is the wing span, f is the parasite area of the aircraft and e is Oswald's efficiency factor of the aircraft.

This formulation deviates from the standard convention, which represents the aerodynamic parameters in a coefficient form. This representation was adopted in order to allow us to analyze the dependence of the results on the various aircraft's parameters. Carson's work was published before the UAV era, and refers to small manned aircraft only. An assumption in this study is that the above lift to drag ratio will still hold for most fixed-wing UAV's, due to their similar general structure to small manned aircraft.

Equations (17) through (19) may not be good approximations for the real dependence of drag-to-lift on speed when the Reynolds number is small, or when the UAV's structure is irregular. This problem is avoided in the case of constant airspeed, where D/L is constant and results are presented in the form of the *relative* amount of fuel/battery capacity that is saved. This is a result of the fact that energy consumption can be shown to be proportional to the D/L ratio, with or without the presence of wind.

In cases where the speed-dependent drag-to-lift ratio of the UAVs can be expressed in a more accurate form (e.g., based on experiments), this form should replace the generalized ratio in equation (17) to achieve more realistic results.

The optimal lift-to-drag ratio occurs when eq. (17) reaches its minimum value. If the dependence of the engine's efficiency on the aircraft's speed is ignored, the flight speed that produces the optimal lift to drag ratio becomes [3]

$$(20) \quad V^{opt} = \left(\frac{B}{A} \right)^{1/4} = (2W)^{1/2} (\rho^2 b^2 f \pi e)^{-1/4},$$

and the optimal lift to drag ratio is:

$$(21) \quad \left(\frac{D}{L} \right)^{opt} = 2\sqrt{AB} = 2\sqrt{\frac{f}{\pi b^2 e}}.$$

In the arc optimization analysis, where the optimal flight within individual arcs is found, the objective function is defined as the total amount of energy spent over the given arc. This objective function is measured in Joules as well as the objective function of the network-scale shortest path optimization. Both of them need to be minimized, starting with the arc optimization.

For a zero-wind scenario, the total energy spent, or the *cost* of crossing an arc (i, j) assuming constant speed and steady wind along the arc is given by eq. (22).

$$(22) \quad cost_{ij} = \frac{\text{Energy spent to resist air drag}}{\text{Engine's efficiency}} = \frac{\text{Air Drag Force} \cdot \text{Distance flown}}{\text{Engine's efficiency}},$$

where the engine's efficiency is defined here for a constant speed per unit time:

$$(23) \quad \text{Engine's efficiency} \equiv \eta_{\text{engine}} = \frac{\text{Energy dissipated to the air through direct drag}}{\text{Potential energy in fuel or battery}}.$$

The last equality in eq. (22) emerges from the assumption of constant wind, i.e., constant drag force D along the arc (i, j) , with length X_{ij} :

$$(24) \quad \int_{\text{arc}(i,j)} D(x)dx = DX_{ij}.$$

All of the processes that lead to loss of energy, including drag, will eventually be translated to heating of the environment. Air drag is the main process of energy transfer from the engine to the outside world for reasonably efficient UAVs. Hence, this study introduces the engine's efficiency as a parameter that compensates for the non drag-related processes.

Both the drag forces and the engine's efficiency are functions of the airspeed. Using the fact that the aircraft's weight equals its lift, the energy cost can be expressed as:

$$(25) \quad cost_{ij} = DX_{ij}\eta_{\text{engine}}^{-1} = WX_{ij}\left(\frac{D}{L}\right)\eta_{\text{engine}}^{-1} = mgX_{ij}\left(\frac{D}{L}\right)\eta_{\text{engine}}^{-1}.$$

Assuming constant engine efficiency, for simplicity, and using Carson's optimal speed from equation (20) yields:

$$(26) \quad cost_{ij}^{\text{opt}} = WX_{ij}\left(\frac{D}{L}\right)_{(V_{\text{opt}})}\eta_{\text{engine}}^{-1} = 2WX_{ij}\sqrt{\frac{f}{\pi b^2 e}}\eta_{\text{engine}}^{-1}.$$

2. Effect of Wind

Up to this point, Carson's formulation was used for the case of zero wind. This formulation can be easily transformed to the case of one-dimensional wind, by adding the wind velocity to the UAV's air velocity, to achieve the drag-to-lift ratio in terms of the ground velocity. The next step is to construct a generalized result for $cost_{ij}$ and $cost_{ij}^{opt}$, for the case of a three-dimensional wind velocity. This is necessary for our three-dimensional network representation of wind, paths and waypoints in the various optimization models.

The effect of wind can be regarded as a shift in the frame of reference of the UAV by the wind velocity. This effect leads to a different distance traveled in the earth's frame of reference, compared to the one perceived by the UAV in its flight through the wind. This study assumes that flying through a changing wind field will not cause instabilities, such as the case may be for micro UAVs in turbulence.

The network will be divided into sufficiently small enough arcs to assume a constant wind along an arbitrary arc (i, j) . Let \vec{V}_{ij} be the UAV's velocity in Earth's frame of reference, \vec{V}_{wind} be the wind's velocity in Earth's frame of reference and \vec{V}_{Rel} be the UAV's air velocity, i.e., its velocity in the wind's frame of reference. Therefore,

$$(27) \quad \vec{V}_{Wind} + \vec{V}_{Rel} = \vec{V}_{ij}$$

The angles β and γ_{ij} are defined as the direction of the wind and the arc (i, j) respectively, on a common plane relative to a common arbitrary axis. The direction of flight in the wind's frame of reference is constrained to lead to the next node j , and is denoted by α . In other words, the UAV's air velocity is chosen to be on the plane created by the wind velocity and the line that connects node i to j , and its size and direction are chosen such that the UAV ends up at j . This is illustrated in Figure 13.

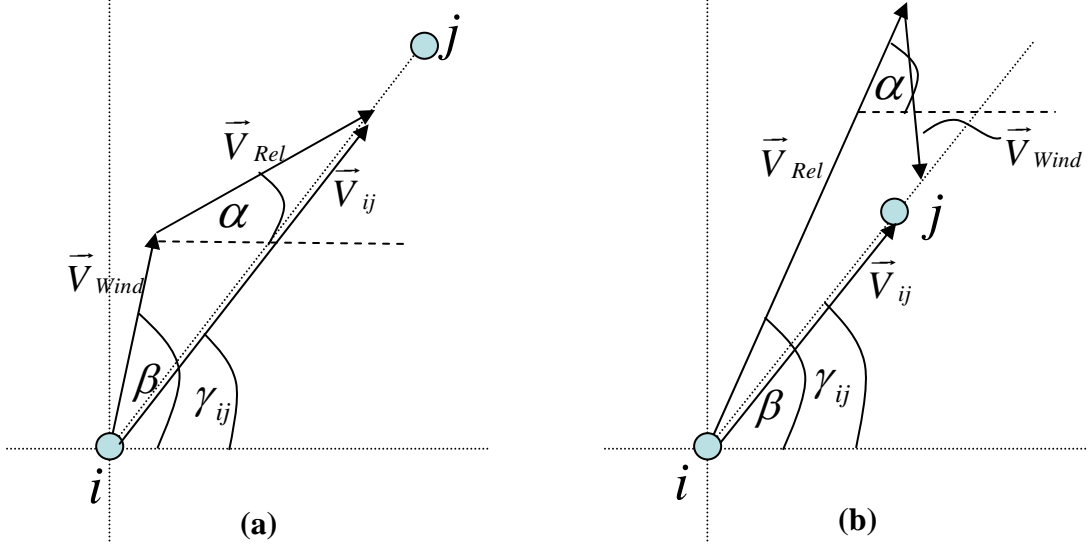


Figure 13. Wind, air and ground velocities (\vec{V}_{wind} , \vec{V}_{Rel} and \vec{V}_{ij} respectively) and the corresponding angles β , α and γ_{ij} with respect to the horizon, on the plane created by \vec{V}_{wind} and \vec{V}_{ij} . Two cases are presented for clarification: (a) Tail wind (b) Head wind.

The total travel distance that the UAV “experiences” in the frame of reference of the wind, X_{Rel} can be expressed as:

$$(28) \quad X_{Rel} = V_{Rel} \cdot t_{ij} = V_{Rel} \frac{X_{ij}}{V_{ij}}$$

Here, $V_{Rel} \equiv |\vec{V}_{Rel}|$, $V_{ij} \equiv |\vec{V}_{ij}|$ are the airspeed and the ground speed, respectively. t_{ij} is the flight time between i and j , and X_{ij} is the true ground distance between i and j . With this in hand, the travel cost can be expressed as:

$$(29) \quad \begin{aligned} cost_{ij} &= W \cdot \eta_{engine}^{-1} \cdot V_{Rel} \cdot \frac{X_{ij}}{V_{ij}} \cdot \left(\frac{D}{L} \right)_{V_{Rel}} = \\ &= W \cdot \eta_{engine}^{-1} \cdot V_{Rel} \cdot \frac{X_{ij}}{V_{ij}} \cdot \left[A V_{Rel}^2 + B / V_{Rel}^2 \right] \end{aligned}$$

The ground speed between i and j , V_{ij} , can be found by vector calculations:

$$(30) \quad V_{ij} = V_{Wind} \cdot \cos(\beta - \gamma_{ij}) + \sqrt{V_{Rel}^2 - V_{Wind}^2 \sin^2(\beta - \gamma_{ij})},$$

where $V_{Wind} \equiv |\vec{V}_{Wind}|$.

V_{ij} depends only on the scalar difference between β and γ_{ij} , which justifies the two dimensional treatment of the wind and arc vectors on the plane that contains them. V_{Rel} is the only controllable variable in this analysis, and it will be chosen to minimize the following expression for the cost:

$$(31) \quad cost_{ij}^{opt} = \underset{V_{Rel}}{MIN} \left\{ \frac{W \cdot \eta_{engine}^{-1} \cdot V_{Rel} \cdot X_{ij} \cdot [A V_{Rel}^2 + B / V_{Rel}^2]}{V_{Wind} \cdot \cos(\beta - \gamma) + \sqrt{V_{Rel}^2 - V_{Wind}^2 \sin^2(\beta - \gamma)}} \right\}$$

where the engine's efficiency, η_{engine} , may be given as a function of the airspeed

In the case of a constant flight speed, this will not be a minimization function, and the only controlled variable will be the direction of flight, α , which can be calculated after observing that (see Figure 13):

$$(32) \quad V_{Wind} \cdot \sin(\beta - \gamma) = V_{Rel} \cdot \sin(\gamma - \alpha),$$

or

$$(33) \quad \alpha = \gamma - \arcsin\left(\frac{V_w}{V_{rel}} \sin(\beta - \gamma)\right).$$

Again, α is measured relative to the horizon on the plane defined by β and γ_{ij} .

Practically, a flight direction α can be achieved dynamically by the control systems of the UAV, given that it is able to aim to the next waypoint j through its navigation system, and correct deviations from the $i - j$ line when needed.

3. Constraints on Airspeed

There are four constraints on the UAV's airspeed, which are developed in this section. Any aircraft's airspeed is limited from below by its stall velocity, V_{Stall} , under

which the lift force becomes too low to resist the aircraft's weight. Hence, our *first constraint* will be: $V_{\text{Rel}} > V_{\text{Stall}}$. Practically, this constraint needs to be further restricted to a higher bound for the airspeed, in order to keep the UAV well on the safe side, above its stall speed.

The *second constraint* is found by ensuring that the UAV is able to overcome the wind and fly on the path from i to j . This is found through geometry, as shown in Figure 14. This constraint is divided into two cases:

- a) If $|\beta - \gamma_{ij}| \leq 90$, then $V_{\text{Rel}} \geq V_{\text{Wind}} |\sin(\beta - \gamma_{ij})|$.
- b) If $|\beta - \gamma_{ij}| > 90$, then $V_{\text{Rel}} \geq V_{\text{Wind}}$.

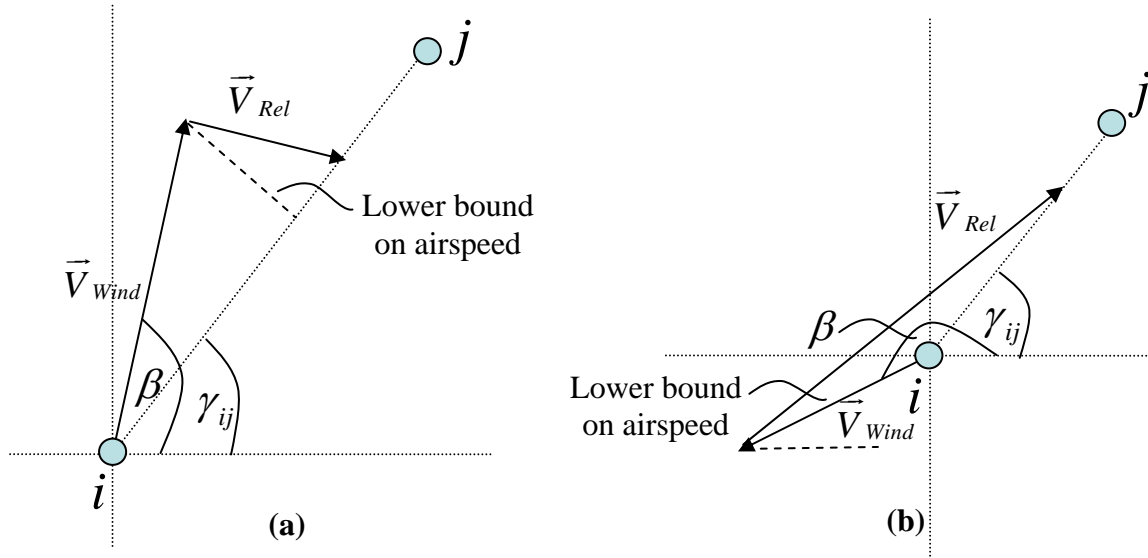


Figure 14. Finding the lower bounds on the airspeed, $|\vec{V}_{\text{Rel}}|$, using geometry, for two cases: **(a)** $|\beta - \gamma_{ij}| \leq 90$ and **(b)** $|\beta - \gamma_{ij}| \geq 90$.

The *third constraint* will be another lower-bound on the UAV's ground speed, which ensures that the UAV will cross any arc in a reasonable time, or in terms of ground speed: $V_{ij} \geq V_{\text{min}}$, where V_{min} is the lowest allowable ground speed. This constraint can be

expressed in terms of V_{Rel} and V_{Wind} because \vec{V}_{ij} is simply the projection of \vec{V}_{Rel} on the path $i - j$ plus the projection of \vec{V}_{Wind} on that path. Altogether:

$$V_{\text{Wind}} \cos(\beta - \gamma) + \sqrt{V_{\text{Rel}}^2 - V_{\text{Wind}}^2 \sin^2(\beta - \gamma)} \geq V_{\text{min}},$$

or in terms of V_{Rel} :

$$V_{\text{Rel}} \geq \sqrt{V_{\text{min}}^2 - 2V_{\text{min}} V_{\text{Wind}} \cos(\beta - \gamma) + V_{\text{Wind}}^2}$$

The *fourth constraint* arises from the limitations of the engine and takes the form $V_{\text{Rel}} \leq V_{\text{max}}$, where V_{max} is the maximal achievable airspeed of the aircraft.

The objective function for the arc cost and the constraints on the UAV's airspeed can be summarized as the following non-linear programming problem:

$$c_{ij} \equiv \text{cost}_{ij}^{\text{opt}} = \underset{V_{\text{Rel}}}{\text{MIN}} \left\{ \frac{W \cdot \eta_{\text{engine}}^{-1} \cdot V_{\text{Rel}} \cdot X_{ij} \cdot [A V_{\text{Rel}}^2 + B / V_{\text{Rel}}^2]}{V_{\text{Wind}} \cdot \cos(\beta - \gamma) + \sqrt{V_{\text{Rel}}^2 - V_{\text{Wind}}^2 \sin^2(\beta - \gamma)}} \right\},$$

subject to:

$$V_{\text{max}} \geq V_{\text{Rel}} \geq V^*,$$

where:

$$(34) \quad V^* \equiv \begin{cases} \text{MAX} \left(\frac{V_{\text{Stall}}, V_{\text{Wind}} \left| \sin(\beta - \gamma_{ij}) \right|}{\sqrt{V_{\text{min}}^2 - 2V_{\text{min}} V_{\text{Wind}} \cos(\beta - \gamma) + V_{\text{Wind}}^2}} \right), & |\beta - \gamma_{ij}| \leq 90. \\ \text{MAX} \left(\frac{V_{\text{Stall}}, V_{\text{Wind}}}{\sqrt{V_{\text{min}}^2 - 2V_{\text{min}} V_{\text{Wind}} \cos(\beta - \gamma) + V_{\text{Wind}}^2}} \right), & |\beta - \gamma_{ij}| > 90. \end{cases}$$

4. Turning

The networks implemented in this study measure dozens of kilometers, while the arcs are 1-1.42 km long. It will be shown that with arcs of 1 km length or more, the cost of a turn from arc (i, j) to arc (j, k) is negligible compared to the total cost of crossing the arcs (i, j) and (j, k) . To show that the cost of turns is negligible in the models of this

study, a simplified model for turns is considered with the following assumptions: (a) turns are made along a circular arc, and (b) turns are characterized by a constant radial acceleration and a constant absolute speed.

A turn from arc (i, j) to arc (j, k) starts with velocity \vec{V}_1 and ends with velocity \vec{V}_2 , such that $|\vec{V}_1| = |\vec{V}_2|$ under assumption (b). The radius of the turn is R , and its radial angle θ , as illustrated in Figure 15.

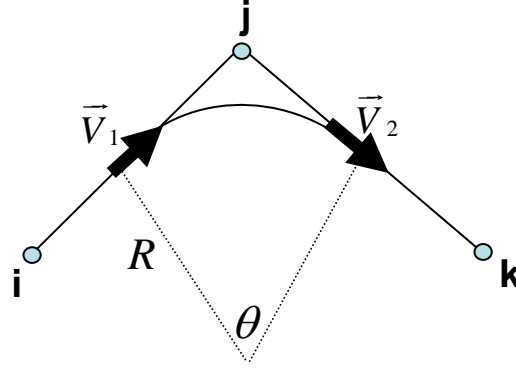


Figure 15. A circular turn from arc (i, j) to arc (j, k) , with turn radius R , over θ degrees.

A turn is achieved by producing a radial acceleration through the aerodynamic forces created by the UAV's wings. In a two dimensional turn, the horizontal projection of the lift on the line that connects the UAV and the center of the desired turn circle equals to the radial force. For every extra unit of force that is taken from the lift for the purpose of turning, an extra $D/L \cdot \eta_{engine}^{-1}$ units of thrust need to be produced by the engine. During a turn, the UAV must use a roll angle, δ , to create a projection of the lift on the horizontal plane. Therefore, the extra energy spent during a turn, ΔE_{ijk} , is approximated as:

$$\begin{aligned}
(35) \quad \Delta E_{ijk} &= \int \vec{F}_{turn} d\vec{l} = m \left(\frac{D \sin \delta}{L \eta_{engine}} \right) \int \vec{a}_{turn} d\vec{l} = \kappa \int \vec{a}_{turn} d\vec{l} = \kappa \vec{a}_{turn} \int d\vec{l} \\
&\approx \kappa \vec{a}_{turn} R \Theta = \kappa \frac{|\Delta V|}{\Delta t} R \Theta = \frac{\kappa |\Delta V| R \Theta}{\Theta / \omega} = \frac{\kappa |\Delta V| R \Theta}{\Theta / (|V| / R)} = m \left(\frac{D \sin \delta}{L \eta_{engine}} \right) |V| |\Delta V|,
\end{aligned}$$

with the following definitions:

$$\kappa \equiv m \left(\frac{D \sin \delta}{L \eta_{engine}} \right), \quad |V| \equiv |V_1| = |V_2| \quad \text{and} \quad |\Delta V| \equiv |\vec{V}_1 - \vec{V}_2|.$$

The fourth equality in eq. (35) is a result of the constant acceleration assumption, and the fifth equality is a result of the circular turn assumption.

The ratio between ΔE_{ijk} and the cost of crossing arc (i, j) can be calculated by dividing eq. (35) by eq. (25):

$$(36) \quad \left(\frac{\Delta E_{ijk}}{\text{cost}_{ij}} \right)^{MAX} \approx \frac{m \left(\frac{D \sin \delta}{L \eta_{engine}} \right) |V| |\Delta V|}{mg X_{ij} \left(\frac{D}{L \eta_{engine}} \right)} = \frac{\sin \delta |V| |\Delta V|}{g X_{ij}}.$$

The largest angles in the network are 109.5 degrees (e.g., flying to an upper-right corner and returning to the lower left corner in the next 9-nodes layer). This corresponds to a maximum of $|\Delta V| = 1.63|V|$. The steepest roll angles needed for a turn from arc to arc will be bounded from above by $\delta = 30$ degrees, assuming long turns (over hundreds of meters). Therefore, the maximal energy ratio is:

$$(37) \quad \left(\frac{\Delta E_{ijk}}{\text{cost}_{ij}} \right)_{MAX} < \frac{0.82 |V|^2}{g X_{ij}}.$$

Since $|V|$ is usually in the order of 20-25 m/s and $1 \leq X_{ij} \leq 1.42$ km, this ratio will be lower than:

$$\frac{0.82 \times 25^2}{9.81 \cdot 1000} = 5.22\%$$

in most cases, and hence, neglected in this work. The price of considering turns in the models of this study is compromising the exact or approximate algorithms in chapter IV, for heuristic ones. An exact algorithm that considers turns would have required multiplying nodes in every location by the number of possible turns to these nodes, which may significantly slow the calculations, and hence, is not done in this work.

5. Climbing and Descending

The cost of vertical movement between two altitudes h_i and h_j is approximated as the original $cost_{ij}$ added to the difference in the potential energies, $mg(h_j - h_i)$. Under the assumptions that excess energy cannot be transferred between arcs due to the speed control, and that climbing / descending angles are shallow⁴, the modified cost becomes:

$$(38) \quad cost_{ij}^{Climb/Descend} = cost_{ij} + MAX \{mg(h_j - h_i), 0\}.$$

Steep climbing angles may change the drag to lift ratio for a given speed, which makes climbing and descending a non-symmetric processes in terms of the extra energy that is consumed or gained, in addition to the basic arc cost [29] However, our use of small vertical angles keeps eq. (38) in a simple form.

6. Effect of Flight Altitude

In general, the following effects can be identified with the addition of the vertical degree of freedom for flight:

- A higher altitude means a lower air density, and a different drag to lift ratio.
- Better wind directions or speeds may be found at higher or lower altitudes, similarly to the benefit of a horizontal degree of freedom. In general, the higher the altitude, the higher the wind speeds.

The effect of the change in air density is discussed in this section.

⁴ In this study, the climbing or descending angles are bounded by roughly 5.7 degrees, since the vertical layers separation is 100 m, and the minimum horizontal separation is 1000 m.

In eq. (18) and eq. (19) for the lumped parameters A and B , the fact that the air density ρ is a function of the altitude h , was stressed. The models in this thesis use the following approximation in eq. (39) for the air density [32]:

$$(39) \quad \rho(h) = \frac{Mp(h)}{RT(h)} = \frac{M}{R} \frac{p_0 \left(1 + \frac{Lh}{T_0}\right)^{-\frac{gM}{RL}}}{T_0 + Lh},$$

where:

p_0 is the sea level atmospheric pressure [Pa],

T_0 is the sea level standard temperature [K],

L is the temperature lapse rate [K/m],

R is the universal gas constant [J/mol/K],

M is the molecular weight of dry air [kg/mol].

Use of the UAV parameters in Table 2, zero wind and an arc length of 1 km yields the cost function in Figure 16.

Table 2. Representative values for a small UAV

Parameter	Symbol	Value
Mass [kg]	m	5
Wind span [m]	b	1.93
Parasite area [m ²]	f	0.028
Oswald's factor	e	0.7
Engine's efficiency	η	0.7

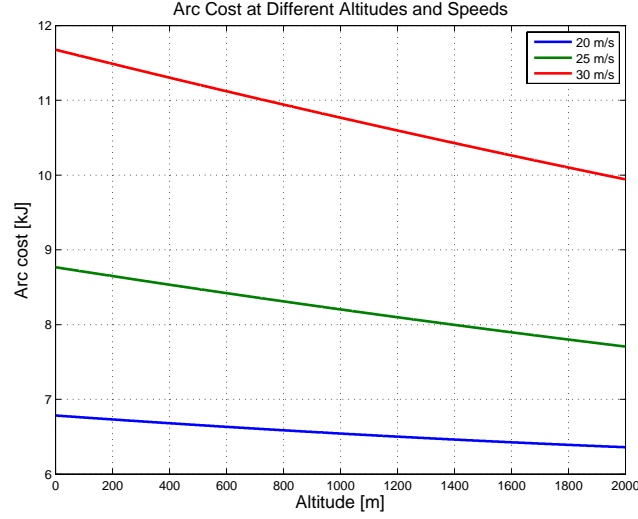


Figure 16. Arc costs at altitudes up to 2000 m, for three different flight speeds, with the UAV parameters given in Table 2.

Figure 16 illustrates that the cost function decreases with altitude almost linearly for the entire relevant range. In sections IV.B and IV.C this fact is used to shorten the computation time when complex algorithms or when large networks are involved. This will be done by the use of tables and fitting, instead of repeatedly solving the constrained nonlinear optimization problems in eq. (34).

E. ESTIMATION OF UAV PARAMETERS

In order to simulate representative UAVs of different masses, according to the different models (see Chapter IV), the following approximation for the wing span is used:

$$(40) \quad b \approx 1.041 \cdot m^{0.382},$$

where b is the wing span in meters and m is the takeoff mass, in kilograms.

Oswald's efficiency factor was taken to be 0.7 and the parasite surface area, f , is approximated through the wing span:

$$(41) \quad f \propto \left(\frac{b}{10}\right)^2,$$

which approximately coincides, for example, with Rascal UAV ($b \approx 2.4m$, $f \approx 0.054m^2$) [14].

Results of the simulations are given in the form of the ratio between the energy cost of the suggested paths, compared to the energy cost of the straight-line path with a constant flight velocity. Therefore the engine's efficiency η_{engine} that appears as an inverse factor in the nonlinear minimization program for the arc cost (eq. (34)) will have no significance for the results.

IV. NETWORK-SCALE OPTIMIZATION

A. CHAPTER OVERVIEW

This chapter discusses the construction of five network models for minimum-energy paths and compares their energy conservation performance. The five network models are (1) a deterministic model that assumes perfect knowledge of the atmosphere and provides an upper bound on the optimal energy saving for comparison with the other more realistic models, (2) a stochastic-static model that assumes the use of forecasts only and provides a pre-flight plan, (3) a stochastic-dynamic model that takes into account real-time measurements by the GPS-INS, (4) an improved stochastic-dynamic model that considers the correlation structure of the atmosphere, and (5) a maximum-duration model that is based on the stochastic-dynamic shortest path and provides an optimized ratio between flight duration and energy consumed.

B. MODEL I: DETERMINISTIC SHORTEST PATH

The deterministic shortest-path model uses statistical knowledge about the given wind forecast to create a realistic scenario. Dijkstra's shortest-path algorithm [31] is then used to find the path with the minimum energy cost from origin s to destination t . This corresponds to the ideal case, where complete information about the network is given, and serves as an upper bound on the optimal energy saving for the other models.

The deterministic shortest-path model is solved after computing the cost and speed to fly for each arc in the network using the constrained non-linear programming model in eq. (34). For faster calculations, finding the arc costs may also be done through the use of a table for the direct translation of wind velocity to an arc cost and a suggested speed to fly, based on the non linear program in eq. (34). Since the cost function depends also on the altitude, this study proposes using a linear interpolation of two tables, for two extreme flight altitudes at the lower and upper potential flight levels. The example in Figure 16 demonstrates that a linear behavior will be a good approximation between sea

level and 2000 m. It should be noted that different tables must be constructed for each UAV, as the cost function depends on its physical parameters. An example for such tables is shown in Figure 17.

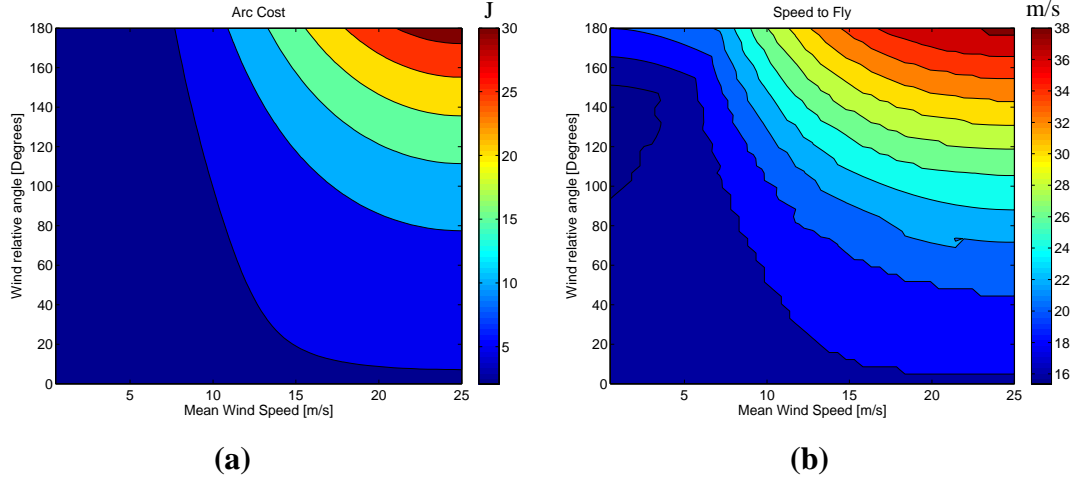


Figure 17. (a) Arc costs [J] and (b) Suggested speed to fly as functions of wind speed and relative wind direction for the UAV parameters in Table 1.

The deterministic shortest-path model uses eq. (10) for one realization of the distribution of wind velocities, given the forecasted components of the wind velocity. For consistency when comparing this model with the other models, the same realizations of wind velocities are used in order to provide a valid upper bound by model I.

The steps for implementing model I are as follows:

1. Construct a network for the flight space, with origin node $s \in N$ and destination node $t \in N$, according to section III.B.
2. Interpolate a forecast in the spatial and temporal domain limits according to section II.E.
3. Create a realization of wind velocities, using eq. (10).
4. For each arc in the network, calculate its cost, according to eq. (34).
5. Calculate the shortest path from s to t using Dijkstra's algorithm [31].

C. MODEL II: STOCHASTIC-STATIC SHORTEST PATH

The stochastic-static shortest-path model uses the statistical behavior of the wind, to calculate the expected (average) arc costs in the network, and use these to find the

shortest path with Dijkstra's shortest path algorithm. This model represents the case of a pre-flight plan, and assumes no updates during the flight. It serves as a lower bound on the optimal energy saving for the stochastic-dynamic model, as it uses only forecast data and no updates of the path during the flight.

The expected arc cost is expressed through the following equation:

$$(42) \quad E[cost_{ij}] = \int_{V_{Wind}=0}^{\infty} \int_{\beta=-\pi}^{\pi} cost_{ij} \left\{ V_{Wind}, \varphi \left[\vec{V}_{Wind} (\beta + \beta_0), \vec{X}_{ij} \right] \right\} g(\beta) f(V_{Wind}) d\beta dV_{Wind},$$

where $cost_{ij}$ is the arc cost, as in eq. (34), given as a function of the wind speed $V_{Wind} = |\vec{V}_{Wind}|$ and its relative direction to the arc (i, j) vector \vec{X}_{ij} . β_0 is the average direction of the wind, and β is the fluctuation around it, that follows a normal distribution $g(\beta)$ as in eq. (9). φ is the relative angle between \vec{X}_{ij} and the fluctuating wind velocity, \vec{V}_{Wind} . The wind speed follows a Weibull distribution $f(V_{Wind})$, as in eq. (1).

For strong enough head winds, no feasible solution could be found to the constrained nonlinear program, since a minimum ground speed would not be achieved. Therefore, the integration limits are reduced into the range of two standard deviations below and above the average wind speed and direction, using σ_v and σ_β respectively, as shown in eq. (43). For the wind direction β , the distribution is normal and hence, this approximation “skips” 4.55% of the range of angles in the integration, for a range of two standard deviations around the mean (i.e., there is a 4.55% chance to encounter wind directions outside the range of the integral). The wind speed follows Weibull distribution which has the cumulative distribution in eq. (2). Figure 18 shows that the resulting reduction in the range of integration of the approximation is quite low, in the order of 4.5%. The relation between the average wind speed and its standard deviation is found through eq. (10).

$$\begin{aligned}
(43) \quad E[cost_{ij}] &= \\
&= \int_{\bar{V}_{Wind}-2\sigma_V}^{\bar{V}_{Wind}+2\sigma_V} \int_{\beta_0-2\sigma_\beta}^{\beta_0+2\sigma_\beta} cost_{ij} \left\{ V_{Wind}, \varphi \left[\bar{V}_{Wind} (\beta + \beta_0), \bar{X}_{ij} \right] \right\} g(\beta) f(V_{Wind}) d\beta dV_{Wind}.
\end{aligned}$$

where \bar{V}_{Wind} is the average wind speed.

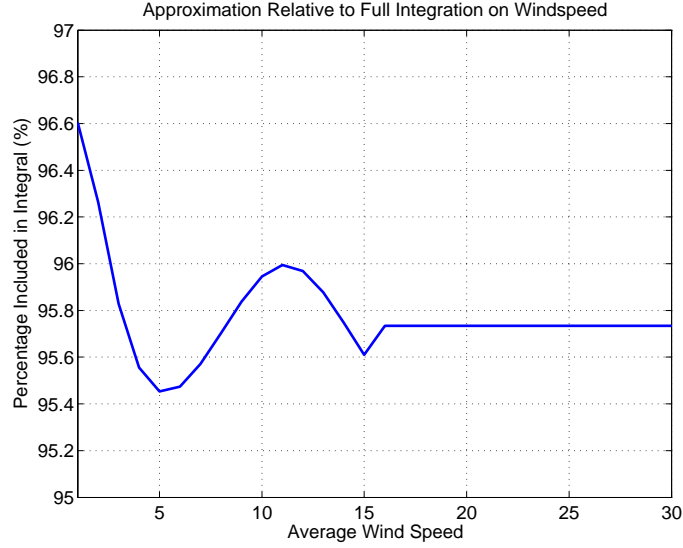


Figure 18. Comparison of approximation (43) to the full integral in eq. (42), regarding the range of integration over wind speeds.

The expressions within the integrals may produce infeasible solutions. In order to avoid averaging of solutions that include infeasible airspeeds, the constraints of eq. (34) are first ignored. Then, whenever the solution for the unconstrained nonlinear program is higher than the maximum allowed airspeed, the maximum airspeeds will be used as the speed to fly, and the high cost functions will serve as penalties. That way, arcs that can usually be crossed with a legitimate flight speed (under non-extreme wind velocities) will remain available on one hand, but penalized with high cost on the other hand. Figure 19 illustrates such a situation, where flight speeds are bounded by 38 m/s, and the corresponding cost of solutions that may require speeds higher than that are penalized.

Since eq. (34) solves a non-linear program for each value of β and V_{Wind} in the range of the double integral, it will be computationally expensive to solve it in real-time for every arc in the network. There are two efficient ways of calculating the expected cost:

1. Draw enough random realizations from $g(\beta)$ and $f(V_{Wind})$ to estimate the average.
2. Construct a table for the average cost for every combination of V_{Wind} and φ , and use a linear interpolation for the dependency on the flight altitude, as described in Model I.

The first method will be used when comparing the three models, due to the fact that a set of realizations for the random fluctuations of the wind (defined by V_{Wind} and φ) are already available from model III (see next section). This study suggests using the second method in real-time calculations.

The suggested speed to fly will be the expected best speed to fly, for the entire range of realizations from $g(\beta)$ and $f(V_{Wind})$. This may not be the optimal choice for the flight speed, but serves as a representative value for it. In this model, no information on the real wind velocity will be measured during the flight. Thus, the exact optimal flight speed is unknown. Figure 19 shows the results for the average arc cost and suggested speeds to fly for a specific UAV.

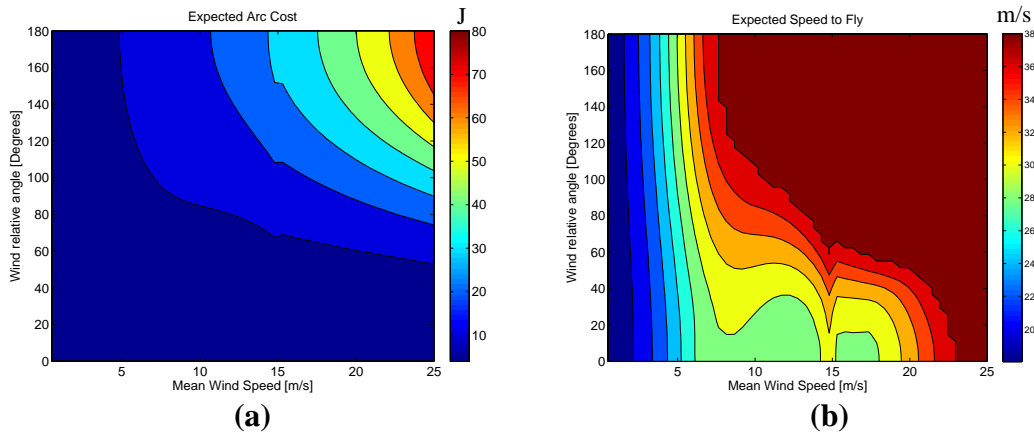


Figure 19. (a) Expected arc costs [J] and (b) Expected speed to fly as functions of wind speed and relative wind direction for the UAV parameters in Table 1.

The steps of implementing model II are as follows:

1. Construct a network for the flight space, with origin S and destination T, according to section III.B.
2. Interpolate a forecast according to section II.E.,
3. Option A:
 - 1) Create a large set of realization of wind velocities, using eq. (10).
 - 2) For each arc in the network calculate its set of realized costs according to eq. (34) and take their average to obtain the expected arc costs.
 - 3) Penalize costs for unfeasible solutions, as shown in Figure 19.
 Option B:
 - 1) Create a table of expected arc costs and speeds to fly, using eq. (43).
 - 2) Penalize costs for unfeasible solutions, as shown in Figure 19.
4. Calculate the shortest path from s to t using the expected arc costs and Dijkstra's algorithm [31].

D. MODEL III: STOCHASTIC-DYNAMIC SHORTEST PATH

The stochastic-dynamic shortest-path model uses an iterative approximate dynamic programming algorithm that provides the expected path cost from each node to the destination node. This algorithm dynamically re-optimizes the UAV's route based on dynamically collected information about the local wind field. The algorithm used is based on [32] (See also [34]). Arc costs are given as random variables based on the distributions of the wind velocities. When UAV reaches a node, it measures the local wind realization, and infers the cost of each of the neighboring arcs (in its forward star). Then, it makes a decision where to go next based on the measured arc costs and the expected cost-to-go (cost until the destination node) for each of the neighboring nodes. The expected cost-to-go on node i is denoted by V^i . Bellman's equation [33] gives the optimality condition for the V^i 's. In terms of our network formulation, Bellman's equation translates into:

$$(44) \quad V^i = E \left[\min_j \left(V^j + cost_{ij} \right) \right],$$

where $j \in \{l \mid (i, l) \in A\}$ are the neighbors of node i in its forward star [33]. Here, the expectation E is used since the arc cost is a random variable that has an infinite number of potential realizations. Therefore, the model provides the path with the minimum *expected* energy cost.

Solving V^i for every node in the network would be possible in a deterministic scenario, using recursion from the destination node backwards. In the case of discrete distribution for the arc costs, it may also be possible to solve eq. (44) exactly by recursion. In our case, the cost function has a continuous distribution, and an exact solution for eq. (44) cannot be computed in finite computing time. Therefore, this study uses a Monte-Carlo based algorithm with the converging cost-to-go estimates in eq. (46), see below, to replace eq. (44). The expected cost-to-go is iteratively updated with a randomly generated realization of the on-board wind velocity measurement. Iterations terminate upon reaching a reasonable approximation of the expected cost-to-go. Two examples for the convergence of V^i , where i is the origin node, are plotted in Figure 20. In both cases, the initial error is no more than 0.5% of the total cost. Convergence into the range of 0.03% is achieved after 20 iterations.

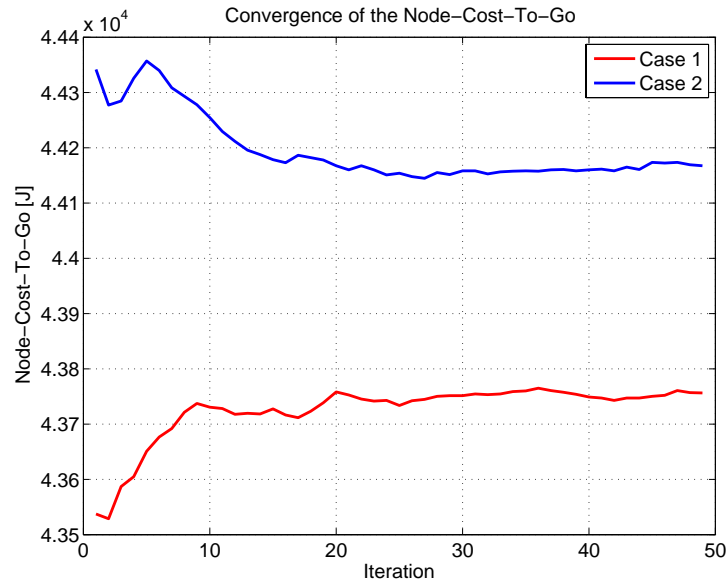


Figure 20. The expected cost-to-go convergence of the origin nodes in two sets of network realizations.

Measurement errors in the dynamic estimation of the local wind velocity are simulated through the use of available data in the literature regarding the accuracy of GPS-INS systems [37]-[40] and estimations for the case where compass corrections for the UAV's "crab angle" are available [14].

Another type of error that is taken into account is the "Spatial fluctuation error." It represents the different wind velocities at different points along the arcs emanating from the node where the measurement was made. The error is calculated as the variation in wind velocities for the collection of all adjacent node pairs in the forecast, including on the diagonals. The histograms of the variations in speed and direction between neighboring nodes are plotted in Figure 21. These variations are added as errors to the measurements by the GPS-INS system as they represent the difference between local wind velocities and the wind velocities along neighboring arcs.

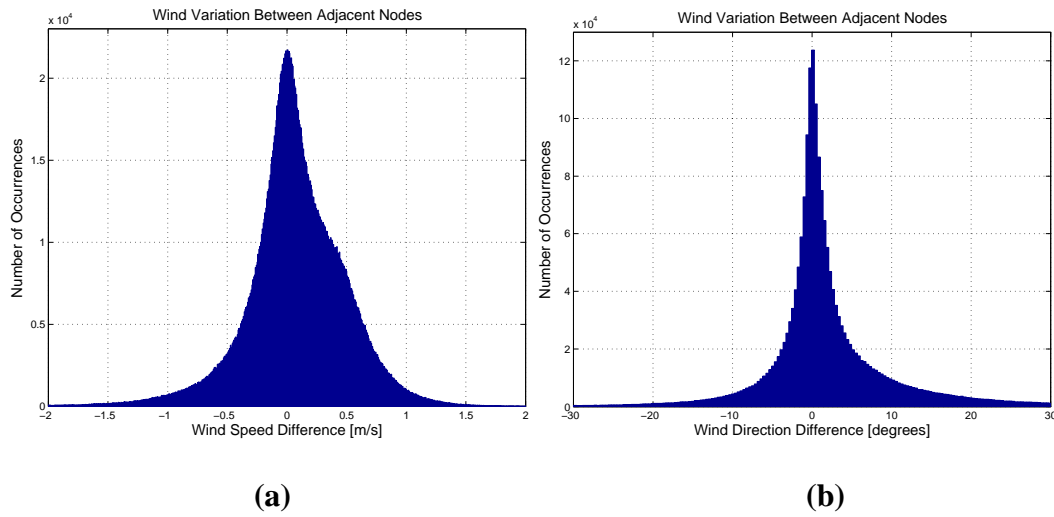


Figure 21. Wind variation between adjacent nodes in terms of (a) wind speed and (b) wind direction.

Errors in the estimation of wind speed and direction are assumed to have a Normal distribution with a standard deviation that equals to the root sum squares (RSS) of the two types:

$$(45) \quad \sigma_{estimate}^i = \sqrt{\sigma_{GPS-INS}^i{}^2 + \sigma_{Fluctuations}^i{}^2},$$

where i stands for either speed or direction, $\sigma_{estimate}$ is the total estimation error, $\sigma_{GPS-INS}$ is the standard deviation of the GPS-INS error, and $\sigma_{fluctuations}$ is the standard deviation of the spatial fluctuations. Table 3 summarizes the data on measurement errors and spatial fluctuations, collected from the Marina weather station and COAMPS forecasts.

Table 3. Estimation errors of wind speed and direction in the form of standard deviations

Parameter (standard deviations)	Symbol	Value
Speed Measurement Error [m/s]	$\sigma_{GPS-INS}^{speed}$	2
Speed Spatial Fluctuation Error [m/s]	$\sigma_{fluctuation}^{speed}$	0.7
Total Speed Error [m/s]	$\sigma_{estimate}^{speed}$	2.1
Direction Measurement Error [degrees]	$\sigma_{GPS-INS}^{direction}$	10
Direction Spatial Fluctuation Error [degrees]	$\sigma_{fluctuation}^{direction}$	5
Total Direction Error [degrees]	$\sigma_{estimate}^{direction}$	11.2

The steps of implementing model III are as follows:

1. Construct a network for the flight space, with origin s and destination t , according to section III.B.
2. Interpolate a forecast according to section II.E.
3. Start with an initial guess for the expected cost-to-end, V_0^i , for every node i in the network, e.g., using the results of model II to find the cost of the shortest path over the expected values of the arc costs, from each node i to the destination t .
4. Create a large set of $n \gg 1$ realization of wind velocities, using eq. (10).
5. For each realization, with index $k \in \{1, \dots, n\}$, calculate the cost of every arc $(i, j) \in A$, $cost_{ij}^k$, according to eq. (34) using a sample of the wind velocity on arc (i, j) .
6. For every node i in the network, update the value of V_{k-1}^i to V_k^i as follows:

$$(46) \quad V_k^i = (1 - \alpha_k) \underset{j}{\text{Min}} [V_{k-1}^j + \text{cost}_{ij}^k] + \alpha_k V_{k-1}^i,$$

where α_k serves as a weighting factor, that can be computed in various ways. To achieve an arithmetic mean at every iteration k , use:

$$(47) \quad \alpha_k = \frac{1}{k+1}.$$

7. Repeat stage 6 for the n realizations. Figure 20 illustrates the rate of convergence of V^s .

Now the model is ready for a flight with dynamic measurements:

1. Start at node s .
2. Measure the real arcs costs $\text{cost}_{ij}^{\text{real}}$ from the current node i to the adjacent nodes j , for $(i, j) \in A$.
3. Fly to node l that satisfies:

$$(48) \quad l = \underset{j}{\text{Argmin}} [V_n^j + \text{cost}_{ij}^{\text{real}}].$$
4. Repeat stages 2-3 until reaching the destination node t .

In a simulation, stages 2-3 use arc costs with random measurement errors according to Table 3.

E. MODEL IV: CORRELATION-BASED STOCHASTIC-DYNAMIC SHORTEST PATH

This model uses the spatial and temporal correlation structure of the atmosphere, as described in section II.F, to achieve reduced energy consumption. This model assumes a spatially-autocorrelated joint distribution for the wind velocities, instead of independent marginal distributions as was assumed in the previous models. This model relates only to the correlation structure of the *fluctuations* around the forecasted quantities. The model is similar to model IV, with the difference that measurements give us new information about wind in the entire space of flight, and not only on the adjacent arcs. As noted in section II.F, the temporal and spatial correlation structure of the atmosphere is not available at the time of the study, not even for a specific region, and may require experimentation or construction of a physical theory.

The model uses techniques for creating correlated wind velocities, through correlated normal and Weibull distributions (see [41],[42] and Appendix) for the wind direction and speed, given a correlation structure of the wind for the relevant ranges of space and time (see section II.F for examples of one-dimensional correlation structures).

The steps of implementing model IV are as follows:

1. Construct a network for the flight space, with origin s and destination t , according to section III.B.
2. Interpolate a forecast according to section II.E.,
3. Start with an initial guess for the nodes-costs-to-end, V_0^i , for every node i in the network.
4. Start at node s .
5. Create a large set of n realization of *correlated* wind velocities from current node onwards, towards the destination, using eq. (10). Create correlated wind speeds and correlated wind directions separately, according to the Appendix. Then combine them into a general wind velocity.
6. For each realization, with index $k \in \{1, \dots, n\}$, calculate the cost of every arc $(i, j) \in A$, $cost_{ij}^k$, according to (34).
7. Choose the largest subset of the realizations $p \in P \subset \{1 \dots n\}$ such that the costs of the neighboring arcs to the current node are within a pre-defined environment ε of the corresponding measured arcs costs, e.g., within $\varepsilon=5\%$ ⁵.
8. Using the subset of realizations in 7, update the value of V_p^i according to (46) for every node i between the current node and the destination, over $|P|$ iterations, as described in model III.
9. After updating the V_p^i 's, choose the next node to fly to, according to (48) and the measurements, and repeat stages 7 and 8 until reaching the destination t .

⁵ In a high resolution network, all of the nine neighboring arcs should have a similar wind velocity, both in the measurements and in the created set of realizations, due to the high correlation of wind velocity between adjacent arcs.

F. MODEL V: MAXIMUM DURATION STOCHASTIC-DYNAMIC SHORTEST PATH

The maximum duration stochastic-dynamic shortest path model is based on the stochastic-dynamic model. It also assumes a flight between origin s and destination t . Instead of minimizing energy per distance, it maximizes the flight time per unit energy (e.g., hours of flight per gallon of fuel, or minimizes energy per unit time). This model follows the steps of model III exactly, except for one difference: the energy cost function in eq. (34) is divided by X_{ij}/V_{ij} , to obtain energy per unit time:

$$(49) \quad \begin{aligned} cost_{ij}^{opt} &= MIN_{V_{Rel}} \left\{ W \cdot \eta_{engine}^{-1} \cdot \left[A V_{Rel}^3 + B / V_{Rel} \right] \right\}, \\ &\text{subject to:} \\ &V_{max} \geq V_{Rel} \geq V^*. \end{aligned}$$

where V^* is defined as in eq. (34).

Let E_{ij} be the energy cost of crossing arc (i, j) and T_{ij} be the time to cross arc (i, j) . Define Λ and $\bar{\Lambda}$ be as:

$$(50) \quad \Lambda = Min_{all\ paths} \frac{\sum_{(i,j) \in path} E_{ij}}{\sum_{(i,j) \in path} T_{ij}},$$

and:

$$(51) \quad \bar{\Lambda} = Min_{all\ paths} \sum_{(i,j) \in path} \frac{E_{ij}}{T_{ij}}.$$

Solving eq. (49) and applying a shortest-path algorithm will not yield an exact solution, or a solution that converges to the exact one, as in models I-IV. Instead of providing the path with the minimum energy per unit time, Λ , by solving eq. (50), the algorithm solves the approximate expression in eq. (51), to find the path with the minimum sum of the ratios E_{ij}/T_{ij} , $\bar{\Lambda}$. Hence, this is a heuristic algorithm that doesn't necessarily provide the overall best achievable ratio of energy per unit time. This arises from the fact that the

energy to reach from origin to destination can be directly translated into energy per unit distance, but not into energy per unit time, due to the space-based architecture of the network. Despite that, this is a heuristic algorithm it still produces a significant increase in the flight duration per fixed energy.

G. RESULTS

The first three models were implemented in MATLAB, using COAMPS weather forecasts over a 160 km by 160 km region at Yucca Air Force Test Site, Nevada. A total of 1000 North-South and East-West paths of 40 km round trips (approximately 20 km ingress and 20 km egress) were simulated through a Monte Carlo numerical simulation. Horizontal movement was constrained by the network architecture to 5 km, and vertical movement was constrained to be within 500 m. Origins and destinations were chosen randomly under the constraint that they laid no less than 100 m above the highest terrain features in the area of flight. The resulting network contains 1120 nodes and 5980 arcs. Each of the models produced a suggested path to fly and an associated energy cost, which was compared to the energy cost of a straight-line flight.

In the following discussion, all energy savings are computed relative to energy consumption of a straight line flight path from origin to destination with a constant flight speed. Significant energy savings were achieved in head-winds scenarios, in which the models produced complex paths that tried to avoid unfavorable strong currents. Conversely, the models did not produce significant energy savings in tail-wind scenarios, as the suggested paths were similar to the straight-line paths. An example for these observations is shown in Figure 22. The forecasted horizontal component of the wind velocity, V_x , is shown as a contour plot in the background.

Figure 23 compares the energy savings achieved by the deterministic, stochastic-static and stochastic-dynamic models, as a function of the average wind speed along the direct s - t path. As expected, the deterministic model provides an upper bound on the energy saving for the other models. The stochastic-dynamic model produces energy savings as good as the deterministic model, within less than 10% tolerance. This performance is significantly better than the stochastic-static model. The latter model

produced energy savings of no more than 10%. For a 100 kg UAV, the stochastic-dynamic model produced an average improvement (i.e., reduction) of 15.1% in the energy consumption compared to the straight-line paths, and an average improvement of 30.1% in windy cases, in which the average wind speeds were higher than 15 m/s. In general, the higher the wind speeds the better the energy conservation that the models produce, compared to the straight-line flight.

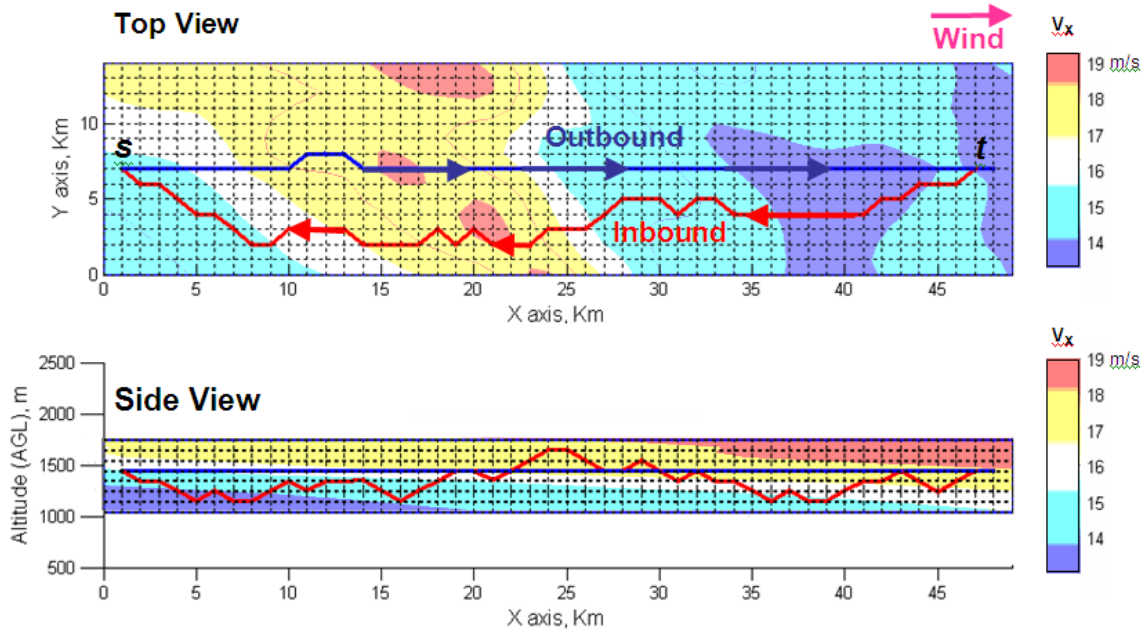


Figure 22. Illustration of a 100 km long round trip from top and side views of the suggested path to fly, using model III.

Figure 24 shows the raw results for the stochastic-dynamic model (model III) without averaging them for similar wind speeds as in Figure 23. It is observed that the variation in the results around the average values is significantly higher for a 10 kg UAV compared to a 100 kg UAV. This translates to a higher predictability in the case of heavier UAVs.

The maximum duration model was simulated without the horizontal degrees of freedom, to represent a border-patrol-like scenario, in which the flight must follow a long

and narrow area. Results for 1000 flights are shown in Figure 25. Best results are achieved for wind speeds between 10 m/s and 15 m/s, in the range of 20-80% increase in the flight duration, compared to a non-optimized flight.

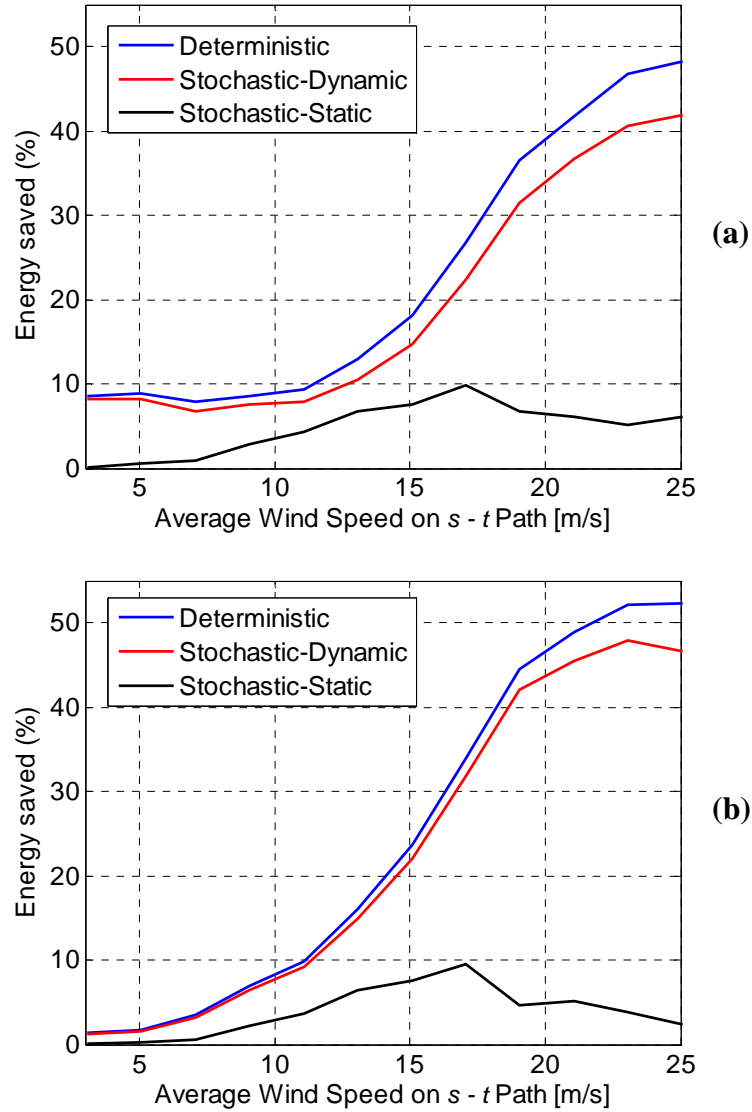


Figure 23. Averaged results from 1000 flight simulations, comparing the energy consumption of paths suggested by models I, II and III to the straight-line path with constant speed, as a function of the average wind speed along the direct $s-t$ path, for two UAV masses: (a) 10 kg and (b) 100 kg.

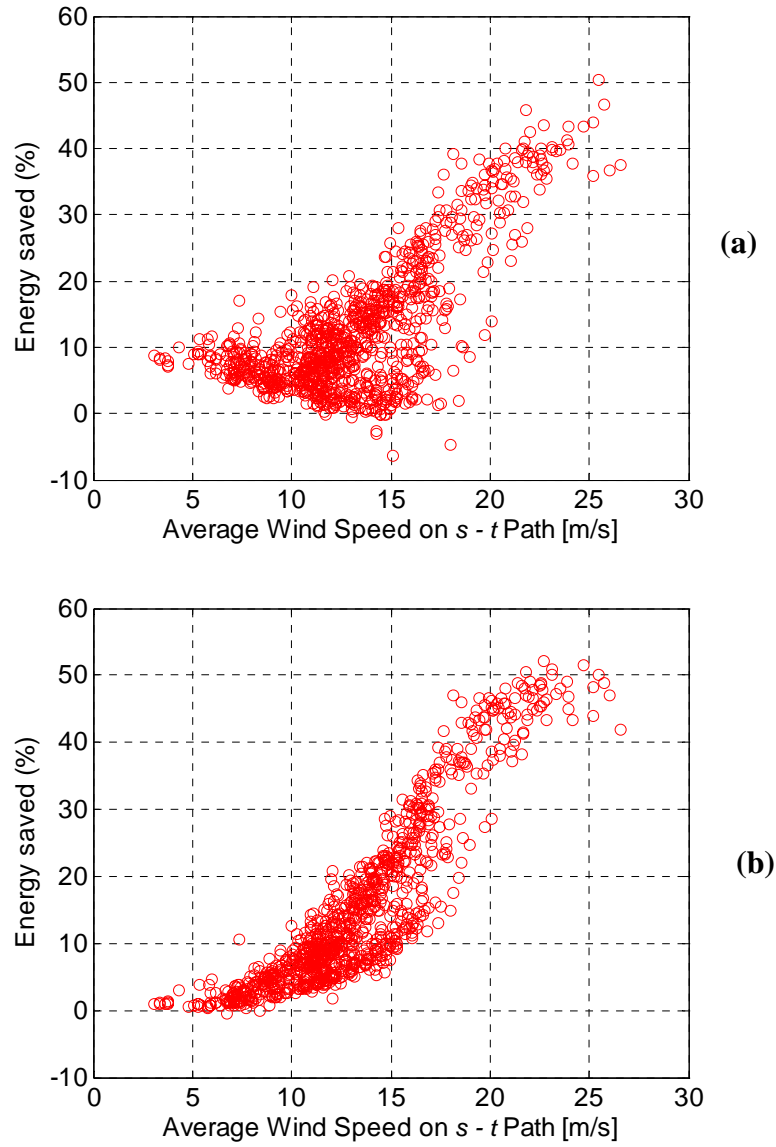


Figure 24. Results from 1000 flight simulations, comparing the energy consumption of model III (Stochastic-Dynamic shortest path) to the straight line-path with constant speed, as a function of the average wind speed along the $s-t$ path, for two UAV masses: (a) 10 kg and (b) 100 kg.

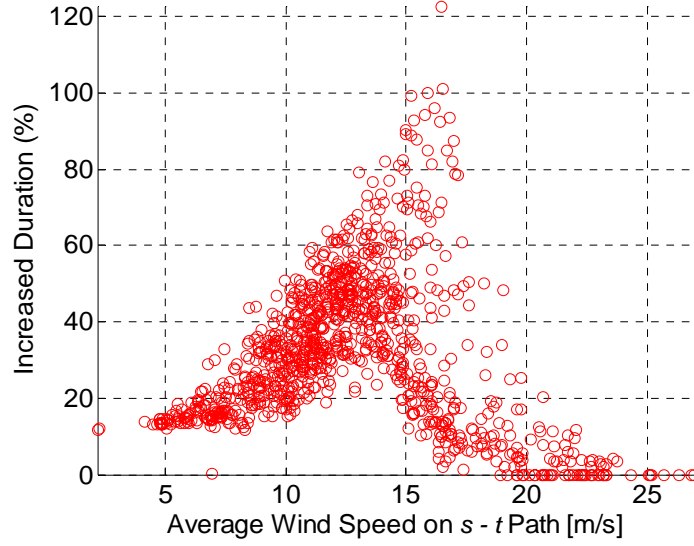


Figure 25. Results from 1000 flight simulations, comparing the increased flight duration per unit energy of model V (Stochastic-Dynamic Maximum Duration path) to the straight line-path with constant speed, as a function of the average wind speed along the $s-t$ path, for a 100 kg UAV.

THIS PAGE INTENTIONALLY LEFT BLANK

V. CONCLUSIONS AND RECOMMENDATIONS

A. CONCLUSIONS

The goal of this thesis is to provide a quantitative analysis of the potential energy savings for unmanned aerial vehicles (UAVs) through the use of wind currents. This thesis has demonstrated a significant average improvement of 30% in energy consumption and flight endurance of UAVs, through network optimization of flight paths and the use of mesoscale weather forecasts with dynamic measurements.

Five optimization models were constructed—four for the minimum-energy path and one for the maximum duration path. The minimum-energy models produced significant energy savings, especially when strong head winds exist and should be avoided. When strong tail winds exist, the optimal flight path is usually very similar to the straight-line path and the models do not produce any significant improvement. Pre-flight path plans, based on weather forecasts, were shown to be inadequate for achieving significant energy saving. With the use of dynamic measurements of wind velocities throughout the flight, the model produces significantly better results that are much closer to the upper bound of energy saving given complete wind knowledge. Therefore, a stochastic-dynamic shortest-path model is recommended for implementation in UAV flights, both in operations and training. This model will realize the triple benefits of (1) conservation of fuel and battery, (2) achievement of longer flight distance and duration, and (3) improved operational flexibility.

B. SUGGESTED WORK AHEAD

There are several interesting scopes to be extended from this thesis. The first immediate step would be to implement and verify the models and algorithms on an actual UAV platform. This can be achieved through collaboration between NPS and the U.S. Naval Research Laboratory. This work item will require modification of existing control software in order to implement Model III: Stochastic Dynamic shortest-path.

The second work item would be to expand the existing models to handle more complex flight patterns, in addition to the simple origin-destination operations assumed in this thesis.

The third work item would be to collect data on the spatial and temporal correlation structure of the wind. Such data collection is required for the implementation of Model IV: Correlation based Stochastic Dynamic shortest-path. This model is expected to provide better performance than the Model III: Stochastic Dynamic shortest-path.

The fourth work item would be to conduct sensitivity analysis of the algorithm performance with respect to aerodynamics and environmental conditions. Aerodynamic variables should include mass, wing span, parasite surface area and Oswald's efficiency factor. Environmental conditions should include flight distance, flight altitude, terrain features (hilly versus flat), network size and discretization level. The last two conditions contribute to the vertical and horizontal degrees of freedom for flight. However, they increase the computation time of the algorithms and hence should be balanced appropriately.

APPENDIX.

Creation of approximately correlated random variables (RVs) with Normal and Weibull distributions given their correlation structure, can be done in the following ways (based on [41] for Normal RVs and on [42] for Weibull RVs).

Creation of Correlated RVs with Normal Distribution:

Let $X = (X_1, \dots, X_n) \sim MVN(0, \Sigma)$ be a random vector with a multi-variate normal distribution (MVN) with mean 0 and covariance matrix Σ . Since Σ is symmetric positive definite, it can be expressed using Cholesky decomposition as: $\Sigma = C^T C$, where $C = \sqrt{D}U$ such that D is a diagonal matrix with positive elements, and U is an upper triangular matrix. The way to generate $X = (X_1, \dots, X_n) \sim MVN(M, \Sigma)$ is as follows:

1. Generate a vector $Y = (Y_1, \dots, Y_n) \sim MVN(0, I)$ of n independent RVs, with mean 0 and standard deviation 1.
2. Find C , the Cholesky decomposition matrix of Σ .
3. $X = M + C^T Y$ is the required set of correlated RVs.

Creation of Correlated RVs with Weibull Distribution (Approximation):

The way to generate $X = (X_1, \dots, X_n) \sim MVW(\mu, \sigma, \rho)$, where $\mu = (\mu_1, \dots, \mu_n)$ are the averages, $\sigma = (\sigma_1, \dots, \sigma_n)$ are the standard deviations and ρ is the $n \times n$ correlation matrix is as follows:

1. Define an $n \times 1$ vector V , such that: $V_i = \frac{\sigma_i}{\mu_i}$
2. Define the matrix ρ^* through its elements:

$$\begin{aligned} \rho_{ij}^* = & 1.063 - 0.004\rho_{ij} - 0.001\rho_{ij}^2 - 0.2(V_i + V_j) + 0.337(V_i^2 + V_j^2) + \\ & + 0.007\rho_{ij}(V_i + V_j) - 0.007V_i V_j \end{aligned}$$

3. Define $\bar{\rho} \equiv \rho^* \rho$

4. Create $Y = (Y_1, \dots, Y_n) \sim MVN(0, \bar{\rho})$ as described above for correlated Normal RVs.

5. Let: $k_i = \left(\frac{\sigma_i}{\mu_i} \right)^{-1.086}$, $c_i = \frac{\mu_i}{\Gamma\left(1 + \frac{1}{k_i}\right)}$, as defined for the two parameters of Weibull

distribution in equations (6) and (7).

6. $X_i = \left\{ -\log[1 - \Theta(Y_i)] \right\}^{\frac{1}{k_i}} c_i$ is the required multi variate vector of correlated RVs,

where the cumulative Normal distribution $\Theta(Y_i)$ defined as:

$$\Theta(Y_i) = \frac{1}{\sqrt{2\pi}\sigma} \int_{-\infty}^{Y_i} e^{-\frac{t^2}{2\sigma^2}} dt$$

LIST OF REFERENCES

- [1] FM 3-04.155, "Army Unmanned Aerial Operations," Headquarters, Department of the U.S. Army, April 2006.
- [2] J.M. Abatti, "Small Power: The Role of Micro and Small UAVs in the Future," Air Command and Staff College, 2005.
- [3] B.H. Carson, "Fuel Efficiency of Small Aircraft," U.S. Naval Academy, Annapolis, AIAA-80-1847, 1980.
- [4] S. Caselli, M. Regianni, R. Rocchi, "Heuristic Methods for Randomized Path Planning in Potential Fields," University of Parma, Italy, 2001.
- [5] J.S.B. Mitchell, D.M. Keirsey, "Planning Strategic Paths through Variable Terrain Data," in *Proceeding of the SPIE Conference on Applications of Artificial Intelligence*, Vol. 485, Arlington, VA, 1984, pp. 172-179.
- [6] D. Rathbun, S. Kragelund, A. Pongpunwattana and B. Capozzi, "An Evolution Based Path Planning Algorithm for Autonomous Motion of a UAV through Uncertain Environments," in *1st Unmanned Aerospace Vehicles, Systems, Technologies, and Operations Conference and Workshop*, Portsmouth, VA, 2002.
- [7] D. Jia, "Parallel Evolutionary Algorithms for UAV Path Planning," in *AIAA 1st Intelligent Systems Technical Conference*, Chicago, Illinois, 2004.
- [8] J.C. Rubio and S. Kragelund, "The Trans-Pacific Crossing: Long Range Adaptive Path Planning for UAVs through Variable Wind Fields," in *Digital Avionics Systems Conference*, Vol. 2, pp. 8.B.4 – 81-12, 2003.
- [9] J.H. Cochrane, "MacCready Theory with Uncertain Lift and Unlimited Altitude," in *Technical Soaring*, Vol. 23, pp. 88-96, July 1999.
- [10] Y. Qi, "Energy-Efficient trajectories of unmanned aerial vehicles flying through thermals," *Journal of Aerospace Engineering*, Vol. 18, No. 2, pp. 84-92, 2005.
- [11] Y.J. Zhao, "Minimum fuel powered dynamic soaring of unmanned aerial vehicles utilizing wind gradients," *Optimal Control Applications and Methods*, Vol. 25, pp. 211-233, 2004.
- [12] D.E. Metzger, "Optimal Flight Paths for Soaring Flight," Arizona State University, Tempe, Arizona, 1974.
- [13] N.E. Kahevski, P.A. Ioannou, M.D. Mirmirani "Optimal Static Soaring of UAVs using Vehicle Routing with Time Windows," in *45th AIAA Aerospace Sciences Meeting*, Reno, Nevada, pp. 1927-1939, 2007.

- [14] K. Jones (private communication), 2007.
- [15] R.C.C. Houghton, "Aircraft Fuel Savings in Jet Streams, by Maximizing Features of Flight Mechanics and Navigation," *Journal of Navigation*, Vol. 51, pp. 360-367, 1997.
- [16] A. Nilim, "Algorithms for Air Traffic Flow Management under Stochastic Environments," in *Proceeding of the American Control Conference*, Vol. 4, pp. 3429-3434, 2004.
- [17] K.S. Ro and P.G. Hunt, "Characteristic Wind Speed Distributions and Reliability of the Logarithmic Wind Profile," *Journal of Environmental Engineering*, Vol. 133, No. 3, pp. 313-318, 2007.
- [18] M.N. Sheer, "Estimation of Wind Energy Potentials in Pakistan," Department of Physics University of Balochistan Quetta, 1993.
- [19] M.C. Alexiadis, P.S. Dokopoulos, H.S. Sahsamanoglou, I.M. Manousaridis, "Short-Term Forecasting of Wind Speed and Related Electrical Power," *Solar Energy*, Vol. 63, No. 1, pp. 61-68, 1998.
- [20] A. McFarlane, "Simulating High-Frequency Winds for Long Durations," in *Thirteenth ASME Wind Energy Symposium*, New Orleans, LA, 1994.
- [21] Professor Richard (Dick) Lind, Department of Meteorology, Naval Postgraduate School, 2007.
- [22] M. Ackley et al., "U.S. Wind Profilers, a Review," Federal Coordinator for Meteorological Services and Supporting Research, Washington, D.C., March 1998.
- [23] R. Coulter, "Radar Wind Profiler and RASS Handbook," Climate Research Facility, U.S. Department of Energy, ARM TR-044, January 2005.
- [24] B. Basel, "A Seasonal Statistical Evaluation of COAMPS[®] over the Arabian Gulf Region," *Pure and Applied Geophysics*, Vol. 164, pp. 1747-1764, 2007.
- [25] C. H. Wash, G. Schmeiser, P.M. Pauley "Verification and Evaluation of NOGAPS and COAMPS Analyses and Forecasts for the 24–26 January 2000 East Coast Cyclone," in *18th Conference on Weather Analysis and Forecasting and the 14th Conference on Numerical Weather Prediction*, Ft. Lauderdale, FL, January 2001.
- [26] M.L Long, Ed., "COAMPS Version III Model Description," The Naval Research Laboratory, Monterey, CA, 2003.

- [27] R.A. Pielke, "Mesoscale Meteorological Modeling," Academic Press, San Diego, CA, p. 138, 2002.
- [28] J.E. Nachamkin, "Evaluation of Dispersion Forecasts Driven by Atmospheric Model Output at Coarse and Fine Resolution," *The Journal of Applied Meteorology and Climatology*, 2007.
- [29] Chambers, J.B., Grafton SB. *Aerodynamic Characteristics of Airplanes at High Angles of Attack*. NASA TM 74097, December 1977.
- [30] R.K. Ahuja, T.L. Magnanti, J.B. Orlin, "Network Flows: Theory, Algorithms and Applications," Upper Saddle River: Prentice Hall, 1993, pp. 35-37.
- [31] E. W. Dijkstra, "A Note on Two Problems in Connection with Graphs," *Numerische Mathematik*, Vol. 1, pp. 269-271, 1959.
- [32] "The Chemistry Encyclopedia," April 2007, http://www.chemistrydaily.com/-chemistry/Density_of_air. [Last Accessed December 9, 2007].
- [33] W.B. Powell, "Approximate Dynamic Programming," pp. 3, 20-24, 100, Princeton University, 2006.
- [34] D.P. Bertsekas, "An Analysis of Stochastic Shortest Path Problems," *Mathematics of Operations Research*, Vol. 16, No. 3, 1991.
- [35] J. Rus, "Dynamic Programming," University of Maryland, April 2006.
- [36] "UAV design guidelines," 2007, http://www.barnardmicrosystems.com/L4E_UAV_design.htm. [Last Accessed December 9, 2007].
- [37] Q. Ladetto, B. Merminod, P. Terrier, Y. Schutz, "On Foot Navigation: When GPS Alone is Not Enough," *Journal of Navigation*, Cambridge University Press, Vol. 53, pp. 279-285, 2000.
- [38] X.F. He, Y.Q. Chen, B. Vik, "Design of Minimax Robust Filtering for an Integrated GPS/INS System," *Journal of Geodesy*, Vol. 73, pp. 407-411, 1999.
- [39] M.P. Doukas, "A New Method for GPS-Based Wind Speed Determination during Airborne Volcanic Plume Measurements," U.S. Geological Survey, 2002.
- [40] C.H. Hajiyev, O. Akgun, "Integration of Air Data System and Doppler Radar via Kalman Filtering," *Aircraft Engineering and Aerospace Technology*, Vol. 74, No. 4, pp. 345-354, 2002.

- [41] M. Haugh, "The Monte Carlo Framework, Examples from Finance and Generating Correlated Random Variables," Class Notes for IEOR E4703, Department of Industrial Engineering and Operational Research, Columbia University, Fall 2004.
- [42] O. Ditlevsen and H.O. Madsen, "Structural Reliability Methods," John Wiley & Sons, Chichester, pp. 317-323, 1996. Internet Edition 2.2. Available at <http://www.mek.dtu.dk/staff/od/books.htm>, May 2003. [Last Accessed December 9, 2007].

INITIAL DISTRIBUTION LIST

1. Defense Technical Information Center
Ft. Belvoir, Virginia
2. Dudley Knox Library
Naval Postgraduate School
Monterey, California
3. Professor Johannes O. Royset
Naval Postgraduate School
Monterey, California
4. Professor Kevin Jones
Naval Postgraduate School
Monterey, California
5. Dr. Jason Nachamkin
Naval Postgraduate School
Monterey, California
6. Prof. Richard Lind
Defense Technical Information Center
Ft. Belvoir, Virginia
7. James Ehlert
Naval Postgraduate School
Monterey, California
8. Prof. Karl Pfeiffer
Naval Postgraduate School
Monterey, California
9. Prof. Patricia Jacobs
Naval Postgraduate School
Monterey, California
10. Prof. Moshe Kress
Naval Postgraduate School
Monterey, California
11. Prof. Thomas Hoivik
Naval Postgraduate School
Monterey, California